

A Response to Editor Comments

Dear Dr. Feingold,

Thank you for the corrections and comments on our manuscript (#acp-2018-499). They are greatly appreciated.

We are submitting a revised manuscript for your consideration of publication in *Atmospheric Chemistry and Physics*. We have carefully studied your comments and revised the manuscript accordingly. Please find the response (marked as blue) to the major comments. We have provided a copy of track-change manuscript as well as a clean copy of the revised manuscript.

Thank you for your consideration of this submission. We hope you find our response adequately address your comments and the revision/corrections acceptable. We would greatly appreciate it if you could get back to us with your decision at your earliest convenience.

Sincerely,

Peng Wu

Department of Hydrology and Atmospheric Sciences

University of Arizona

Tucson, AZ 85721, USA

Lines 62-65, 220-223: definition and understanding of autoconversion and accretion.

Thanks for the comments and corrections.

We were trying to say, '*cloud* droplets reach maximum size by *condensation* near cloud top' and autoconversion is dominant at the top part of the cloud layer where cloud droplets collide to form drizzle drops.

To avoid confusion, the definition and interpretation in lines 62-65 and 220-223 have been rephrased:

Lines 62-65 (62-64 in the revision): 'Autoconversion represents the process of drizzle drops being formed through the self-collection of cloud droplets and accretion represents the process where rain drops grow by collecting cloud droplets.'

Lines 220-223 (228-230 in the revision): 'Autoconversion dominates around cloud top where drizzle drops form by the self-collection of cloud droplets and accretion is dominant at middle and lower parts of the cloud where rain drops grow by collecting cloud droplets.'

Lines 193-194: clarify cloud types; line 210: validity of 'adiabatic growth' assumption.

Thanks for this comment.

In line 194 of the revised manuscript, the cloud selection criteria were clarified: 'only single-layered and overcast low-level clouds with $Z_{\text{top}} \leq 3$ km were selected'.

In the retrieval method in Append A, the layer-mean N_c is from Dong et al. (2014a and 2014b), in which only single layered and overcast low-level cloud properties were retrieved. Therefore, the analysis in this study is for stratus and stratocumulus, which makes the adiabatic assumption appropriate when retrieving cloud liquid water content. No cumulus properties are retrieved in this study.

Line 202: reflectivity threshold to identify drizzling clouds

Thank you for the comment.

We added the following to lines 203-210 in the revised manuscript to comment on the reflectivity threshold.

'Note the differences of the reflectivity thresholds used here and in other studies. For example, -15 dBZ in Sauvageot and Omar (1987), -17 dBZ in Frisch et al. (1995), -19 to -16 dBZ in Wang and Geerts (2003) and -30 dBZ or lower in Kollias et al. (2011). The threshold used in this study is set at the cloud base rather than for the entire cloud layer as in the abovementioned studies. The -37 dBZ threshold is a statistical value from WACR observations at the Azores presented by Wu et al. (2015, Figure 2a), in which it is found that using a higher threshold will miss a significant number of drizzling events especially the clouds with virga.'

Lines 517, 531: lognormal distribution for cloud DSD and normalized gamma distribution for rain DSD.

In the retrieval method, cloud drop size distribution (DSD) is assumed to be lognormal distribution and rain DSD is assumed to be normalized gamma distribution, which are the common practice when retrieving cloud (e.g., Frisch et al., 1995; Dong et al., 1997; McFarlane et al., 2003; Fielding et al., 2015) and rain (e.g., O'Connor et al., 2005; Fielding et al., 2015; Posselt et al., 2017) microphysical properties.

The parameter from the retrieval we used is the cloud liquid water content (CLWC) rather than DSD. Frisch et al. (1998) suggested that, given radar reflectivity and a constraint on total liquid water path (LWP), the retrieved CLWC is relatively insensitive to the assumptions about size distribution.

In this study, to be consistent with the Morrison and Gettleman (2008) scheme, the spatial distribution (approximated using temporal distribution) of q_c is fitted using gamma distribution. The lognormal fitting was also performed, and the results are very similar to those from gamma fitting (lines 325-328 in the revision).

References:

- Dong X., Ackerman, T. P., Clothiaux, E. E., Pilewskie, P., and Han, Y.: Microphysical and Radiative Properties of Stratiform Clouds Deduced from Ground-based Measurements, *J. Geophys. Res.*, 102, 23829-23843, 1997.
- Dong, X., Xi, B., Kennedy, A., Minnis, P. and Wood, R.: A 19-month Marine Aerosol-Cloud_Radiation Properties derived from DOE ARM AMF deployment at the Azores: Part I: Cloud Fraction and Single-layered MBL cloud Properties, *J. Clim.*, 27, doi:10.1175/JCLI-D-13-00553.1, 2014a.
- Dong, X., Xi, B., and Wu, P.: Investigation of Diurnal Variation of MBL Cloud Microphysical Properties at the Azores, *J. Clim.*, 27, 8827-8835, 2014b.
- Fielding, M. D., Chiu, J. C., Hogan, R. J., Feingold, G., Eloranta, E., O'Connor, E. J. and Cadetdu, M. P.: Joint retrievals of cloud and drizzle in marine boundary layer clouds using ground-based radar, lidar and zenith radiances. *Atmospheric Measurement Techniques*, 8, pp. 2663-2683. ISSN 1867-8548 doi: 10.5194/amt-8-2663-2015, 2015.
- Frisch, A. S., Fairall, C. W., and Snider, J. B.: Measurement of stratus cloud and drizzle parameters in ASTEX with a Ka-band Doppler radar and a microwave radiometer, *J. Atmos. Sci.*, 52, 2788–2799, 1995.
- Frisch, A. S., Feingold, G., Fairall, C. W., Uttal, T., and Snider, J. B.: On cloud radar and microwave radiometer measurements of stratus cloud liquid water profiles, *J. Geophys. Res.*, 103, 23,195–23,197, 1998.
- McFarlane, S. A., Evans, K. F., and Ackerman, A. S.: A Bayesian algorithm for the retrieval of liquid water cloud properties from microwave radiometer and millimeter radar data, *J. Geophys. Res.-Atmos.*, 107, AAC 12-1–AAC 12-21, <https://doi.org/10.1029/2001JD001011>, 2003.

- Kollias, P., Szyrmer, W., Rémillard, J., and Luke, E.: Cloud radar Doppler spectra in drizzling stratiform clouds:2. Observations and microphysical modeling of drizzle evolution, *J. Geophys. Res.*, 116, D13203, doi:10.1029/2010JD015238, 2011.
- O'Connor, E. J., Hogan, R. J., and Illingworth, A. J.: Retrieving stratocumulus drizzle parameters using Doppler radar and lidar, *J. of Applied Meteorol.*, 44, 14-27, 2005.
- Posselt, D.J., Kessler, J. and Mace, G.G.: Bayesian retrievals of vertically resolved cloud particle size distribution properties. *Journal of Applied Meteorology and Climatology*, 56, 745–765. <https://doi.org/10.1175/JAMC-D-16-0276.1>, 2017.
- Sauvageot, H., and Omar, J.: Radar reflectivity of cumulus clouds, *J. Atmos. Oceanic Technol.*, 4, 264–272, 1987.
- Wang, J., and Geerts, B.: Identifying drizzle within marine stratus with W-band radar reflectivity, *Atmos. Res.*, 69, 1–27, 2003.
- Wu, P., Dong, X. and Xi, B.: Marine boundary layer drizzle properties and their impact on cloud property retrieval, *Atmos. Meas. Tech.*, 8, 3555–3562. doi: 10.5194/amt-8-3555-2015, 2015.

1 **Evaluation of autoconversion and accretion enhancement factors in Ggeneral Ccirculation**

2 **Mmodel warm-rain parameterizations using ground-based measurements at the Azores**

3 Peng Wu¹, *Baiké Xi¹, Xiquan Dong¹, and Zhibo Zhang²

4¹ Department of Hydrology and Atmospheric Sciences, The University of Arizona, Tucson,

5 Arizona, USA

6² Physics Department, The University of Maryland, Baltimore County, Maryland, USA

7

8

9 Submitted to Atmospheric Chemistry and Physics (November 28~~+~~, 2018)

10

11

12 **Keywords:** MBL clouds, enhancement factors, autoconversion and accretion parameterizations

13

14

15

16

17

18* Corresponding author address: Dr. Baiké Xi, Department of Hydrology and Atmospheric

19 Sciences, University of Arizona, 1133 E. James E. Rogers Way, Tucson, AZ 85721-0011.

20 baikexi@email.arizona.edu; Phone: 520-626-8945

21 **Abstract**

22 A great challenge in climate modelling is how to parametrize sub-grid cloud processes, such
23 as autoconversion and accretion in warm rain formation. In this study, we use ground-based
24 observations and retrievals over the Azores to investigate the so-called enhancement factors,
25 E_{auto} and E_{accr} , which are often used in climate models to account for the influences of sub-grid
26 variances of cloud and precipitation water on the autoconversion and accretion processes. E_{auto}
27 and E_{accr} are computed for different equivalent model grid sizes. The calculated E_{auto} values
28 increase from 1.96 (30 km) to 3.2 (180 km), and the calculated E_{accr} values increase from 1.53
29 (30 km) to 1.76 (180 km). Comparing the prescribed enhancement factors in Morrison and
30 Gettleman (2008, MG08) to the observed ones, we found that a higher E_{auto} (3.2) at small grids
31 and lower E_{accr} (1.07) are used in MG08, which ~~helps to~~might explain why most of the GCMs
32 produce too frequent precipitation events but with too light precipitation intensity. The ratios
33 of rain to cloud water mixing ratio at $E_{accr}=1.07$ and $E_{accr}=2.0$ are 0.063 and 0.142, respectively,
34 from observations, further suggesting that the prescribed value of $E_{accr}=1.07$ used in MG08 is
35 too small to simulate ~~correct~~ precipitation intensity correctly. Both E_{auto} and E_{accr} increase when
36 the boundary layer becomes less stable, and the values are larger in precipitating clouds
37 ($CLWP > 75 \text{ gm}^{-2}$) than those in nonprecipitating clouds ($CLWP < 75 \text{ gm}^{-2}$). Therefore, the
38 selection of E_{auto} and E_{accr} values in GCMs should be regime- and resolution- dependent.

39

40 1. Introduction

41 Due to their vast areal coverage (Warren et al., 1986, 1988; Hahn and Warren, 2007) and
42 strong radiative cooling effect (Hartmann et al., 1992; Chen et al., 2000), small changes in the
43 coverage or thickness of marine boundary layer (MBL) clouds could change the radiative
44 energy budget significantly (Hartmann and Short, 1980; Randall et al., 1984) or even offset the
45 radiative effects produced by increasing greenhouse gases (Slingo, 1990). The lifetime of MBL
46 clouds remains an issue in climate models (Yoo and Li, 2012; Jiang et al., 2012; Yoo et al.,
47 2013; Stanfield et al., 2014) and represents one of the largest uncertainties in predicting future
48 climate (Wielicki et al., 1995; Houghton et al., 2001; Bony and Dufresne, 2005).

49 MBL clouds frequently produce precipitation, mostly in the form of drizzle (Austin et al.,
50 1995; Wood, 2005a; Leon et al., 2008; Wood, 2012). A significant amount of drizzle ~~is~~
51 evaporates ~~d~~ before reaching the surface, for example, about ~76% over the Azores region in
52 Northeast Atlantic (Wu et al., 2015), which provides ~~another~~ water vapour source for MBL
53 clouds. Due to their pristine environment and their ~~close vicinity proximity~~ to the surface, MBL
54 clouds and precipitation are especially sensitive to aerosol perturbations (Platnick and
55 Twomey, 1994~~Quaas et al., 2009; Kooperman et al., 2012~~). Thus, accurate prediction of
56 precipitation is essential in simulating the global energy budget and in constraining aerosol
57 indirect effects in climate projections.

58 Due to the coarse spatial resolutions of the general circulation model (GCM) grid, many
59 cloud processes cannot be adequately resolved and must be parameterized. For example, warm
60 rain parameterizations in most GCMs treat the condensed water as either cloud or rain from the
61 collision-coalescence process that is partitioned into autoconversion and accretion sub-
62 processes in model parameterizations (Kessler, 1969; Tripoli and Cotton, 1980; Beheng, 1994;
63 Khairoutdinov and Kogan, 2000; Liu and Daum, 2004). Autoconversion represents the process
64 ~~that of~~ drizzle drops being formed through the self-collection condensation of cloud droplets
65 and accretion represents the process where rain drops grow by ~~the coalescence of drizzle-sized~~
66 ~~drops with~~collecting cloud droplets. Autoconversion mainly accounts for precipitation
67 initiation while accretion primarily contributes to precipitation intensity. Autoconversion is
68 often parameterized as functions of cloud droplet number concentration (N_c) and cloud water
69 mixing ratio (q_c), while accretion depends on both cloud and rain water mixing ratios (q_c and
70 q_r) (Kessler, 1969; Tripoli and Cotton, 1980; Beheng, 1994; Khairoutdinov and Kogan, 2000;
71 Liu and Daum, 2004; Wood, 2005b). The majority of previous studies suggested that these two
72 processes as can be represented by power law functions of cloud and precipitation properties
73 (See section 2 for details).

74 In conventional GCMs, the lack of information on the sub-grid variances of cloud and
75 precipitation leads to the unavoidable use of the grid-mean quantities ($\overline{N_c}$, $\overline{q_c}$, and $\overline{q_r}$, where
76 henceforth overbar denotes grid mean, ~~same below~~) in calculating autoconversion and

77 accretion rates. MBL cloud liquid water path (CLWP) distributions are often positively skewed
78 (Wood and Hartmann, 2006; Dong et al., 2014a and 2014b), that is, the mean value is greater
79 than the mode value. Thus, the mean value only represents a relatively small portion of samples.
80 Also, due to the nonlinear nature of the relationships, the two processes depend significantly
81 on the sub-grid variability and co-variability of cloud and precipitation microphysical
82 properties (Weber and Quass, 2012; Boutle et al., 2014). In some GCMs, sub-grid scale
83 variability is often ignored or hard-coded using constants to represent the variabilities under
84 all meteorological conditions and across the entire globe (Pincus and Klein, 2000; Morrison
85 and Gettleman, 2008; Lebsock et al., 2013). This could lead to systematic errors in precipitation
86 rate simulations (Wood et al., 2002; Larson et al., 2011; Lebsock et al., 2013; Boutle et al.,
87 2014; Song et al., 2018), where GCMs are found to produce too frequent but too light
88 precipitation compared to observations (Zhang et al., 2002; Jess, 2010; Stephens et al., 2010;
89 Nam and Quaas, 2012; Song et al., 2018). The bias is found to be smaller by-when using a
90 probability density function (PDF) of cloud water to represent the sub-grid scale variability in
91 autoconversion parameterization (Beheng, 1994; Zhang et al., 2002; Jess, 2010), or more
92 complexly, by integrating the autoconversion rate over a joint PDF of liquid water potential
93 temperature, and total water mixing ratio (Cheng and Xu, 2009).

94 Process rate enhancement factors (E) are introduced when considering sub-grid scale
95 variability in parameterizing grid-mean processes and they should be parameterized as

96 functions of the PDFs of cloud and precipitation properties within a grid box (Morrison and
97 Gettleman, 2008; Lebsock et al., 2013; Boutle et al., 2014). However, these values in some
98 GCM parameterization schemes are prescribed as constants regardless of ~~underlying~~ surface
99 or meteorological conditions (Xie and Zhang, 2015). Boutle et al. (2014) used aircraft in situ
100 measurements and remote sensing techniques to develop a parameterization for cloud and rain,
101 in which they not only consider the sub-grid variabilities under different grid scales, but also
102 consider the variation of cloud and rain fractions. The parameterization was found to reduce
103 the precipitation estimation bias significantly. Hill et al. (2015) modified this parameterization
104 and developed a regime and cloud type dependent sub-grid parameterization, which was
105 implemented to the Met Office Unified Model by Walters et al. (2017) ~~and-who~~ found that the
106 radiation bias is reduced when using the modified parameterization. Using ground-based
107 observations and retrievals, Xie and Zhang (2015) proposed a scale-aware cloud
108 inhomogeneity parameterization that they applied to the Community Earth System Model
109 (CESM) and found that it can recognize spatial scales without manual tuning and can be applied
110 to the entire globe. The inhomogeneity parameter is essential in calculating enhancement
111 factors ~~and-since they~~ affect the conversion rate from cloud to rain liquid. Xie and Zhang
112 (2015), however, did not evaluate the validity of CESM simulations from their
113 parameterization; the effect of N_c variability or the effect of covariance of cloud and rain on
114 the accretion process was not assessed. Most recently, Zhang et al. (2018) derived the sub-grid

115 distribution of CLWP and N_c from the MODIS cloud product. They also studied the implication
116 of ~~the~~ sub-grid cloud property variations for the simulation of autoconversion-~~rate simulation~~,
117 in particular the enhancement factor, in GCMs. For the first time, the enhancement factor due
118 to the sub-grid variation of N_c ~~is~~was derived from satellite observation, and results reveal
119 several regions downwind of biomass burning aerosols (e.g., Gulf of Guinea, East Coast of
120 South Africa), air pollution (i.e., Eastern China Sea), and active volcanos (e.g., Kilauea Hawaii
121 and Ambae Vanuatu), where the enhancement factor due to N_c is comparable, or even larger
122 than that due to CLWP. However, one limitation of Zhang et al. (2018) is the use of passive
123 remote sensing data only, which cannot distinguish cloud and rain water.

124 Dong et al. (2014a and 2014b) and Wu et al. (2015) reported MBL cloud and rain properties
125 over the Azores and provided the possibility of calculating the enhancement factors using
126 ground-based observations and retrievals. In this study, Aa joint retrieval method to estimate
127 q_c and q_r profiles is proposed based on existing studies (~~and is presented in~~ Appendix A). Most
128 of the calculations and analyses in this study ~~are~~is based on the Morrison and Gettleman (2008,
129 MG08 hereafter) scheme. The enhancement factors in several other schemes are also discussed
130 and compared with the observational results and the approach in this study can be repeated for
131 other microphysics schemes in GCMs. This manuscript is organized as follows: section 2
132 includes a summary of the mathematical formulas from previous studies that can be used to
133 calculate enhancement factors. Ground-based observations and retrievals are introduced in

134 Section 3. Section 4 presents results and discussions, followed by summary and conclusions in
135 Section 5. The retrieval method used in this study is in Appendix A.

136 **2. Mathematical Background**

137 Autoconversion and accretion rates in GCMs are usually parameterized as power law
138 equations (Tripoli and Cotton, 1980; Beheng, 1994; Khairoutdinov and Kogan, 2000; Liu and
139 Daum, 2004):

$$140 \left(\frac{\partial q_r}{\partial t} \right)_{auto} = A \bar{q}_c^{a1} \bar{N}_c^{a2}, \quad (1)$$

$$141 \left(\frac{\partial q_r}{\partial t} \right)_{accr} = B (\bar{q}_c \bar{q}_r)^b, \quad (2)$$

142 where A , $a1$, $a2$, B , and b are coefficients in different schemes listed in Table 1. The \bar{q}_c , \bar{q}_r ,
143 and \bar{N}_c are grid-mean cloud water mixing ratio, rain water mixing ratio, and droplet number
144 concentration, respectively. Because it is widely used in model parameterizations, the detailed
145 results from Khairoutdinov and Kogan (2000) parameterization that has been used in MG08
146 scheme will be shown in Section 4 while a summary will be given for other schemes.

147 Ideally, the covariance between physical quantities should be considered in the calculation
148 of both processes. However, \bar{q}_c and \bar{N}_c in Eq. (1) are arguably not independently retrieved in
149 our retrieval method, which will be introduced in this section and Appendix A. Thus we only
150 assess the individual roles of q_c and N_c sub-grid variations in determining the autoconversion
151 rate. q_c and q_r , on the other hand, are retrieved from two independent algorithms as shown in

152 Dong et al. (2014a and 2014b), Wu et al. (2015) and Appendix A. The effect of the covariance
 153 of q_c and q_r we will assess the effect of cloud and rain property covariance on accretion rate
 154 will be assessed calculations.

155 At the sub-grid scale, the PDFs of q_c and N_c are assumed to follow a gamma distribution
 156 based on observational studies of optical depth in MBL clouds (Barker et al., 1996; Pincus et
 157 al., 1999; Wood and Hartmann, 2006):

$$158 \quad P(x) = \frac{\alpha^\nu}{\Gamma(\nu)} x^{\nu-1} e^{-\alpha x}, \quad (3)$$

159 where x represents q_c or N_c with grid-mean quantity \bar{q}_c or \bar{N}_c , represented by μ , $\alpha = \nu/\mu$ is the
 160 scale parameter, σ^2 is the relative variance of x (= variance divided by μ^2), $\nu = 1/\sigma^2$ is the
 161 shape parameter. ν is an indicator of cloud field homogeneity, with large values representing
 162 homogeneous and small values indicating inhomogeneous cloud fields.

163 By integrating autoconversion rate, Eq. (1), over the grid-mean rate, Eq. (3), with respect
 164 to sub-grid scale variation of q_c and N_c , the autoconversion rate can be expressed as:

$$165 \quad \left(\frac{\partial q_r}{\partial t}\right)_{auto} = A \mu_{q_c}^{a1} \mu_{N_c}^{a2} \frac{\Gamma(\nu+a)}{\Gamma(\nu)\nu^a}, \quad (4)$$

166 where $a = a1$ or $a2$. Comparing Eq. (4) to Eq. (1), the autoconversion enhancement factor
 167 (E_{auto}) can be given with respect to q_c and N_c :

$$168 \quad E_{auto} = \frac{\Gamma(\nu+a)}{\Gamma(\nu)\nu^a}. \quad (5)$$

169 In addition to fitting the distributions of q_c and N_c , we also tried two other methods to
 170 calculate E_{auto} . The first is to integrate Eq. (1) over the actual PDFs from observed or retrieved
 171 parameters and the second is to fit a lognormal distribution for sub-grid variability ~~like whatas~~
 172 has been done in other studies (e.g., Lebsock et al., 2013; Larson and Griffin, 2013). It is found
 173 that all three methods ~~get-provide~~ similar results. In this study, we use a gamma distribution
 174 that is consistent with MG08. Also note that, in the calculation of E_{auto} from \overline{N}_c , the negative
 175 exponent (-1.79) may cause singularity problems in Eq. (5). When this situation occurs, we ~~do~~
 176 ~~perform~~ direct calculations by integrating the PDF of \overline{N}_c rather than using Eq. (5).

177 To account for the covariance of microphysical quantities in a model grid, it is difficult to
 178 apply bivariate gamma distribution due to its complex nature. In this study, the bivariate
 179 lognormal distribution of q_c and q_r is used (Lebsock et al., 2013; Boutle et al., 2014) and can
 180 be written as:

$$\begin{aligned}
 181 \quad P(\overline{q}_c, \overline{q}_r) &= \frac{1}{2\pi\overline{q}_c\overline{q}_r\sigma_{q_c}\sigma_{q_r}\sqrt{1-\rho^2}} \exp \left\{ -\frac{1}{2} \frac{1}{1-\rho^2} \left[\left(\frac{\ln\overline{q}_c - \mu_{q_c}}{\sigma_{q_c}} \right)^2 - 2\rho \left(\frac{\ln\overline{q}_c - \mu_{q_c}}{\sigma_{q_c}} \right) \left(\frac{\ln\overline{q}_r - \mu_{q_r}}{\sigma_{q_r}} \right) + \right. \right. \\
 182 \quad &\left. \left. \left(\frac{\ln\overline{q}_r - \mu_{q_r}}{\sigma_{q_r}} \right)^2 \right] \right\}, \tag{6}
 \end{aligned}$$

183 where σ is standard deviation and ρ is the correlation coefficient of q_c and q_r .

184 Similarly, by integrating the accretion rate in Eq. (2) from Eq. (6), we get the accretion
 185 enhancement factor (E_{accr}) of:

$$186 \quad E_{accr} = \left(1 + \frac{1}{v_{qc}}\right)^{\frac{1.15^2 - 1.15}{2}} \left(1 + \frac{1}{v_{qr}}\right)^{\frac{1.15^2 - 1.15}{2}} \exp(\rho 1.15^2 \sqrt{\ln\left(1 + \frac{1}{v_{qc}}\right) \ln\left(1 + \frac{1}{v_{qr}}\right)}). \quad (7)$$

187 3. Ground-based observations and retrievals

188 The datasets used in this study were collected at the Department of Energy (DOE)
 189 Atmospheric Radiation Measurement (ARM) Mobile Facility (AMF), which was deployed on
 190 the northern coast of Graciosa Island (39.09°N, 28.03°W) from June 2009 to December 2010
 191 (for more details, please refer to Rémillard et al., 2012; Dong et al., 2014a and Wood et al.,
 192 2015). The detailed operational status of the remote sensing instruments on AMF iswas
 193 summarized in Figure 1 of Rémillard et al. (2012) and discussed in Wood et al. (2015). The
 194 ARM Eastern North Atlantic (ENA) site was established on the same island in 2013 and
 195 provides long-term continuous observations.

196 The cloud-top heights (Z_{top}) were determined from the W-band ARM cloud radar (WACR)
 197 reflectivity and only single-layered and overcast low-level clouds with $Z_{top} \leq 3$ km are-were
 198 selected (the detailed selection criteria can be found in Dong et al., 2014a and 2014b). Cloud-
 199 base heights (Z_{base}) were detected by a laser ceilometer (CEIL) and the cloud thickness was
 200 simply the difference between cloud top and base heights. The cloud liquid water path (CLWP)
 201 was retrieved from microwave radiometer (MWR) brightness temperatures measured at 23.8
 202 and 31.4 GHz using a statistical retrieval method with an uncertainty of 20 g m⁻² for CLWP <
 203 200 g m⁻², and 10% for CLWP > 200 g m⁻² (Liljegren et al., 2001; Dong et al., 2000).

204 Precipitating status is identified through a combination of WACR reflectivity and Z_{base} . As in
205 Wu et al. (2015), we labelled the status of a specific time as “precipitating” if the WACR
206 reflectivity below the cloud base exceeds -37 dBZ. Note the differences of the reflectivity
207 thresholds used here and in other studies. For example, -15 dBZ in Sauvageot and Omar (1987),
208 -17 dBZ in Frisch et al. (1995), -19 to -16 dBZ in Wang and Geerts (2003) and -30 dBZ or
209 lower in Kollias et al. (2011). The threshold used in this study is set at the cloud base rather
210 than for the entire cloud layer as in the abovementioned studies. The -37 dBZ threshold is a
211 statistical value from WACR observations at the Azores presented by Wu et al. (2015, Figure
212 2a), in which it is found that using a higher threshold will miss a significant number of drizzling
213 events especially the clouds with virga.

214 The ARM merged sounding data have a 1-min temporal and 20-m vertical resolution below
215 3 km (Trojan, 2012). In this study, the merged sounding profiles are averaged to 5-min
216 resolution. Pressure and temperature profiles are used to calculate air density (ρ_{air}) profiles
217 and to infer adiabatic cloud water content.

218 Cloud droplet number concentration (N_c) is retrieved using the methods presented in Dong
219 et al. (1998, 2014a and 2014b) and are assumed to be constant with height in a cloud layer.
220 Vertical profiles of cloud and rain water content (CLWC and RLWC) are retrieved by
221 combining WACR reflectivity, CEIL attenuated backscatter and by assuming adiabatic growth
222 of cloud parcels water. The A detailed description is presented in Appendix A with the results

223 from a selected case. The CLWC and RLWC values are transformed to q_c and q_r by dividing
224 by air density (e.g., $q_c(z) = CLWC(z)/\rho_{air}(z)$).

225 The estimated uncertainties for the retrieved q_c and q_r are 30% and 18%, respectively (see
226 Appendix A). We used the estimated uncertainties of q_r and q_c as inputs of Eqs. (4) and (7) to
227 assess the uncertainties of E_{auto} and E_{accr} . For instance, $(1 \pm 0.3)q_c$ are used in Eq. (4) and the
228 mean differences are then used as the uncertainty of E_{auto} . ~~The Same~~ method is used to estimate
229 the uncertainty for E_{accr} .

230 The autoconversion and accretion parameterizations ~~partitioned from the collision-~~
231 ~~coalescence process~~ dominate at different levels in a cloud layer. Autoconversion dominates
232 around cloud top where drizzle drops form by the self-collection of cloud droplets ~~droplets~~
233 ~~reach maximum by condensation~~ and accretion is dominant at middle and lower parts of the
234 cloud where rain drops ~~sediment and continue to~~ grow by collecting cloud droplets. ~~Complying~~
235 In accordance with the physical processes, we estimate autoconversion and accretion rates at
236 different levels of a cloud layer in this study. The averaged q_c within the top five range gates
237 (~215 m thick) are used to calculate E_{auto} . To calculate E_{accr} , we use the averaged q_c and q_r
238 within five range gates around the maximum radar reflectivity. If the maximum radar
239 reflectivity appears at the cloud base, then five range gates above the cloud base are used.

240 The ARM merged sounding data are also used to calculate lower tropospheric stability
241 ($LTS = \theta_{700 \text{ hPa}} - \theta_{1000 \text{ hPa}}$), which is used to infer the boundary layer stability. In this study,

242 unstable and stable boundary layers are defined as LTS less than 13.5 K and greater than 18 K,
243 respectively, and an environment with an LTS between 13.5 K and 18 K is defined as mid-
244 stable (Wang et al. 2012; Bai et al. 2018). Enhancement factors in different boundary layers
245 are summarized in Section 4.2 and may be used as references for model simulations. Further,
246 two regimes are classified: CLWP greater than 75 g m^{-2} as precipitating and CLWP less than
247 75 g m^{-2} as nonprecipitating (Rémillard et al., 2012).

248 To evaluate the dependence of autoconversion and accretion rates on sub-grid variabilities
249 for different model spatial resolutions, an average~~d~~ wind speed within a cloud layer was
250 extracted from merged sounding and used in sampling observations over certain periods to
251 mimic different grid sizes in GCMs. For example, two hours of observations corresponds to a
252 72-km horizontal equivalent grid box if mean horizontal in-cloud wind speed is 10 m s^{-1}
253 ~~horizontal wind~~ and if the wind speed is 5 m s^{-1} , four hours of observations ~~is~~are needed to
254 mimic the same horizontal equivalent grid. We used six horizontal equivalent grid sizes (30-,
255 60-, 90-, 120-, 150-, and 180-km) and mainly show the results from 60-km and 180-km
256 horizontal equivalent grid sizes in Section 4. For convenience, we ~~refer use~~ ‘equivalent size’
257 ~~as to imply~~ ‘horizontal equivalent grid size’ from now on.

258 4. Results and discussions

259 In this section, we first show the data and methods using a selected case, followed by
260 statistical analysis based on 19 months of data and multiple time-intervals.

261 4.1 Case study

262 The selected case occurred on July 27, 2010 (Figure 1a) at the Azores. This case was
263 characterized by a long ~~time-period~~ of non-precipitating or light drizzling cloud development
264 (00:00-14:00 UTC) before intense drizzl~~ing~~ occurred (14:00-20:00 UTC). Wu et al. (2017)
265 studied this case in detail to demonstrate the effect of wind shear on drizzle initiation. Here, we
266 choose two periods corresponding to a 180-km equivalent size and having similar mean q_c near
267 cloud top: 0.28 g kg^{-1} for period c and 0.26 g kg^{-1} for period d, but with different distributions
268 (Figures 1c and 1d). The PDFs of q_c are then fitted using gamma distributions to get shape
269 parameters (ν) as shown in Figures 1c and 1d. Smaller ν is usually associated with a more
270 inhomogeneous cloud field, which allows more rapid drizzle production and more efficient
271 liquid transformation from cloud to rain (Xie and Zhang, 2015) in regions that satisfy
272 precipitation criteria, which is usually controlled using a threshold q_r , droplet size or relative
273 humidity (Kessler, 1969; Liu and Daum, 2004). The period d has a wider q_c distribution than
274 the period c, resulting in a smaller ν and thus larger E_{auto} . Using the fitted ν , the E_{auto} from q_c
275 ~~is~~ calculated from Eq. (5) ~~and-for~~ the period d is larger than ~~the-for~~ period c (1.80 vs. 1.33).
276 The E_{auto} values for the ~~periods~~ d and c can also be calculated from N_c using the same procedure
277 as q_c with a similar result (2.1 vs. 1.51). The E_{accr} values for ~~the~~ periods d and c can be
278 calculated from the covariance of q_c and q_r and Eq. (7). Not surprisingly, ~~the~~ period d has
279 larger E_{accr} than ~~the~~ period c. The combination of larger E_{auto} and E_{accr} in ~~the~~ period d

280 contributes to ~~the~~ rapid drizzle production and high rain rate as seen from WACR reflectivity
281 and q_r in Figure A1.

282 It is important to understand the physical meaning of enhancement factors in precipitation
283 parameterization. For example, if we assume two scenarios for q_c with a model grid having the
284 same mean values but different distributions: (1) The distribution is extremely homogeneous,
285 there will be no sub-grid variability because the cloud has the same chance to precipitate and
286 the enhancement factors would be unity (this is true for arbitrary grid-mean q_c amount as well).
287 (2) The cloud field gets more and more inhomogeneous with a broad range of q_c within the
288 model grid box, which results in a greater enhancement factor and increases the possibility of
289 precipitation. That is, a large enhancement factor can make the part of the cloud with higher q_c
290 within the grid box ~~become~~ more efficient in generating precipitation, rather than the entire
291 model grid.

292 Using the LWP retrieved from the Moderate Resolution Imaging Spectroradiometer
293 (MODIS) as an indicator of cloud inhomogeneity, Wood and Hartmann (2006) found that
294 when clouds become more inhomogeneous, cloud fraction decreases, and open cells become
295 dominant, accompanied by ~~with~~ stronger drizzling ~~process~~ (Comstock et al., 2007). The
296 relationship between reduced homogeneity and stronger precipitation intensity ~~is~~ found in this
297 study, ~~which~~ is similar to the findings in other studies (e.g., Wood and Hartmann, 2006,
298 Comstock et al., 2007, Barker et al., 1996; Pincus et al., 1999).

299 It is clear that q_c and N_c in Figure 1b are correlated with each other. In addition to their
300 natural relationships, q_c and N_c in our retrieval method are also correlated (Dong et al., 2014a
301 and 2014b). Thus, the effect of q_c and N_c covariance on E_{auto} is not included in this study. In
302 Figures 1c and 1d, the results are calculated using an equivalent size of 180-km for the selected
303 case on 27 July 2010. In Section 4.2, we will use these approaches to calculate their statistical
304 results for multiple equivalent sizes using the 19-month ARM ground-based observations and
305 retrievals.

306 4.2 Statistical result

307 For a specific equivalent size, e.g. 60-km, we estimate the shape parameter (ν) and calculate
308 E_{auto} through Eqns. (5) and (7). The PDFs of E_{auto} for both 60-km and 180-km equivalent sizes
309 are shown in Figures 2a-2d. The distributions of E_{auto} values calculated from q_c with 60-km
310 and 180-km equivalent sizes (Figures 2a and 2b) are different to each other (2.79 vs. 3.3). The
311 calculated E_{auto} values range from 1 to 10, and most are less than 4. The average value for the
312 60-km equivalent size (2.79) is smaller than that for the 180-km equivalent size (3.2), indicating
313 a possible dependence of E_{auto} on model grid size. Because drizzle-sized drops are primarily
314 ~~resulted from~~formed by the autoconversion, we investigate the relationship between E_{auto} and
315 precipitation frequency, which is defined as the average percentage of drizzling occurrence
316 based on radar reflectivity below ~~the~~ cloud base. Given the average LWP at Azores from Dong
317 et al. (2014b, 109-140 g m⁻²), the precipitation frequency (black lines in Figures 2a and 2b)

318 agrees well with those from Kubar et al. (2009, 0.1-0.7 from their Figure 11). The precipitation
319 frequency within each bin shows an increasing trend for E_{auto} from 0 to 4-6, then oscillates
320 when $E_{auto} > 6$, indicating that in the precipitation initiation process, E_{auto} keeps increasing to a
321 certain value (~ 6) until the precipitation frequency reaches a near-steady state. Higher
322 precipitation frequency ~~Larger E_{auto} values~~ does not necessarily result in larger E_{auto} values
323 ~~higher precipitation frequency~~ but instead may produce more drizzle-sized drops from
324 autoconversion process when the cloud is precipitating.

325 The PDFs of E_{auto} calculated from N_c also share similar patterns of positive skewness and
326 peaks at ~ 1.5 - 2.0 for the 60-km and 180-km equivalent sizes (Figures 2c and 2d). Although the
327 average values are close to their q_c counterparts (2.54 vs. 2.79 for 60-km and 3.45 vs. 3.2 for
328 180-km), the difference in E_{auto} between 60-km and 180-km equivalent sizes becomes large.
329 The precipitation frequencies within each bin are nearly constant or ~~slightly~~ decrease slightly,
330 which are different to their q_c counterparts shown in Figures 2a and 2b. This suggests
331 complicated effects of droplet number concentration on precipitation initiation and warrants
332 more explorations of aerosol-cloud-precipitation interactions. As mentioned in Section 2, q_c
333 and N_c are also fitted using lognormal distributions to calculate E_{auto} . The results are close to
334 ~~those those are close to the results~~ in Figure 2 (not shown here) with average values of 3.28
335 and 3.84, respectively, for 60-km and 180-km equivalent sizes. Because the E_{auto} values
336 calculated from q_c and N_c are close to each other, we will focus on analyzing the results from

337 q_c only for simplicity and clarity. The effect of q_c and N_c covariance, as stated in Section 4.1,
338 is not presented in this study due to the intrinsic correlation in the retrieval (Dong et al., 2014a
339 and 2014b and Appendix A of this study).

340 The covariance of q_c and q_r is included in calculating E_{accr} and the results are shown in
341 Figures 2e and 2f. The calculated E_{accr} values range from 1 to 4 with mean values of 1.62 and
342 1.76 for 60-km and 180-km equivalent sizes, respectively. These two mean values are much
343 greater than the prescribed value used in MG08 (1.07). Since accretion is dominant ~~at-in the~~
344 middle and lower parts of the cloud where rain drops sediment and continue to grow by
345 collecting cloud droplets, we superimpose the ratio of q_r to q_c within each bin (black lines in
346 Figures 2e and 2f) to represent the portion of rain water in the cloud layer. In both panels, the
347 ratios are less than 15%, which means that q_r can be one order of magnitude smaller than q_c .
348 The differences in magnitude are consistent with previous CloudSat and aircraft results (e.g.,
349 Boutle et al., 2014). This ratio increases from $E_{accr}=0$ to ~ 2 , and then decreases, suggesting a
350 ~~possible optimal state for the collision-coalescence process to achieve maximum efficiency for~~
351 ~~converting cloud water into rain water at $E_{accr}=2$. In other words, that~~ the conversion efficiency
352 cannot be infinitely increased with E_{accr} under available cloud water. The ratio of q_r to q_c
353 increases from $E_{accr}=1.07$ (0.063) to $E_{accr}=2.0$ (0.142), indicating that the fraction of rain water
354 in total liquid water using the prescribed E_{accr} is too low. This ratio could be increased
355 significantly using a large E_{accr} value, therefore increasing precipitation intensity in the models.

356 This further ~~proves~~ suggests that the prescribed value of $E_{accr}=1.07$ used in MG08 is too small
357 to correctly simulate precipitation intensity in the models. Therefore, similar to the conclusions
358 in Lebsock et al. (2013) and Boutle et al. (2014), we suggest increasing E_{accr} from 1.07 to 1.5-
359 2.0 in GCMs.

360 To illustrate the impact of using prescribed enhancement factors, autoconversion and
361 accretion rates are calculated using the prescribed values (e.g., 3.2 for E_{auto} and 1.07 for E_{accr} ,
362 MG08; Xie and Zhang, 2015) and the newly calculated ones in Figure 2 that use observations
363 and retrievals. Figure 3 shows the joint density of autoconversion (Figures 3a and 3b) and
364 accretion rates (Figures 3c and 3d) from observations (x-axis) and model parameterizations (y-
365 axis) for 60-km and 180-km equivalent sizes. Despite the spread, the peaks ~~in~~ of the joint
366 density of autoconversion rate appear slightly above the one-to-one line especially for the 60-
367 km equivalent size, suggesting that cloud droplets in the model are more easily to be converted
368 into drizzle/rain drops than in the observations. On the other hand, the peaks ~~of~~ in the accretion
369 rate appear slightly below the one-to-one line, which indicates that simulated precipitation
370 intensities are lower than observed ones. The magnitudes of the two rates are consistent with
371 Khairoutdinov and Kogan (2000), Liu and Daum (2004), and Wood (2005b).

372 Compared to the observations, the precipitation in GCMs occurs at higher frequencies with
373 lower intensities, which might explain why the total precipitation amounts are close to surface
374 measurements over an entire grid box. This ‘promising’ result, however, fails to simulate

375 precipitation on the right scale and cannot capture the correct rain water amount, thus providing
376 limited information in estimating rain water evaporation and air-sea energy exchange.

377 Clouds in an unstable boundary layer have a better chance of getting moisture supply from
378 the surface by upward motion than clouds in a stable boundary layer. Precipitation frequencies
379 are thus different in these two boundary layer regimes. For example, clouds in a relatively
380 unstable boundary layer ~~more easily~~ produce drizzle more easily than those in a stable boundary
381 layer ~~(Wu et al., 2017)~~. ~~Provided~~ Given the same boundary layer conditions, CLWP is an
382 important factor in determining the precipitation status of clouds. At the Azores, precipitating
383 clouds are more likely to have CLWP greater than 75 g m^{-2} than their nonprecipitating
384 counterparts (Rémillard et al., 2012). To further investigate what conditions and parameters
385 can significantly influence the enhancement factors, we classify low-level clouds according to
386 their boundary layer conditions and CLWPs.

387 The averaged E_{auto} and E_{accr} values for each category are listed in Table 2. Both E_{auto} and
388 E_{accr} increase when the boundary layer becomes less stable, and these values become larger in
389 precipitating clouds ($\text{CLWP} > 75 \text{ gm}^{-2}$) than those in nonprecipitating clouds ($\text{CLWP} < 75 \text{ gm}^{-2}$).
390 In ~~real applications~~ model parameterizations, the autoconversion process only occurs when q_c
391 or cloud droplet size reaches a certain threshold (e.g., Kessler, 1969 and Liu and Daum, 2004).
392 Thus, it will not affect model simulations if a valid E_{auto} is assigned to Eq. (1) in a
393 nonprecipitating cloud. The E_{auto} values in both stable and mid-stable boundary layer

394 conditions are smaller than the prescribed value of 3.2, while the values in unstable boundary
395 layers are significantly larger than 3.2, regardless of ~~if-whether~~ they are precipitating ~~or not~~.
396 All E_{accr} values are greater than the constant of 1.07. The E_{auto} values in Table 2 range from
397 2.32 to 6.94 and the E_{accr} values vary from 1.42 to 1.86, depending on different boundary layer
398 conditions and CLWPs. Therefore, as suggested by Hill et al. (2015), the selection of E_{auto} and
399 E_{accr} values in GCMs should be regime-dependent.

400 To properly parameterize sub-grid variabilities, the approaches ~~by-of~~ Hill et al. (2015) and
401 Walters et al. (2017) can be adopted. To use MG08 and other parameterizations in GCMs as
402 listed in Table 1, proper adjustments can be made according to the model grid size, boundary
403 layer conditions, and precipitating status. As stated in the methodology, we used a variety of
404 equivalent sizes. Figure 4 demonstrates the dependence of both enhancement factors on
405 different model grid sizes. The E_{auto} values (red line) increase from 1.97 at an equivalent size
406 of 30 km to 3.15 at an equivalent size of 120 km, which are 38.4% and 2% percent lower than
407 the prescribed value (3.2, upper dashed line). After that, the E_{auto} values remain relatively
408 constant ~~atof~~ ~ 3.18 when the equivalent model size is 180 km, which is close to the prescribed
409 value of 3.2 used in MG08. This result indicates that the prescribed value in MG08 ~~represents~~
410 ~~well-inis appropriate for~~ large grid sizes in GCMs. The E_{accr} values (blue line) increase from
411 1.53 at an equivalent size of 30 km to 1.76 at an equivalent size of 180 km, ~~those-increases~~
412 ~~ofare~~ 43% and 64%, respectively, larger than the prescribed value (1.07, lower dashed line).

413 The shaded areas represent the uncertainties ~~of-in~~ E_{auto} and E_{accr} associated with the
414 uncertainties ~~of-in~~ the retrieved q_c and q_r . When equivalent size increases, the uncertainties
415 ~~slightly~~-decrease slightly. The prescribed E_{auto} is close to the upper boundary of uncertainties
416 except for the 30-km equivalent size, while the prescribed E_{accr} is significantly lower than the
417 lower boundary.

418 It is noted that E_{auto} and E_{accr} depart from their prescribed values ~~in at~~ opposite directions as
419 the equivalent size increases. For models with finer resolutions (e.g., 30-km), both E_{auto} and
420 E_{accr} are significantly different from the prescribed values, which can partially explain the issue
421 of ‘too frequent’ and ‘too light’ precipitation. Under both conditions, the accuracy of
422 precipitation estimation is degraded. For models with coarser resolutions (e.g., 180-km), the
423 average E_{auto} is exactly 3.2 while E_{accr} is much larger than 1.07 when compared to finer
424 resolution simulations. In such situations, the simulated precipitation will be dominated by the
425 ‘too light’ problem, in addition to regime-dependent (Table 2) and as in Xie and Zhang (2015),
426 E_{auto} and E_{accr} should ~~be~~-also be scale-dependent.

427 Also note that the location of ground-based observations and retrievals used in this study is
428 on the remote ocean where the MBL clouds mainly form in a relatively stable boundary layer
429 and are characterized by high precipitation frequency. Even in such environments, however,
430 ~~the~~-GCMs overestimate the precipitation frequency (Ahlgrimm and Forbes, 2014).

431 To further investigate how enhancement factors affect precipitation simulations, we use
432 E_{auto} as a fixed value of 3.2 in Eq. (4), and then calculate the q_c needed for models to reach the
433 same autoconversion rate as observations. The q_c differences between models and observations
434 are then calculated, which represent the q_c adjustment in models to ~~get~~achieve a realistic
435 autoconversion rate in the simulations. Similar to Figure 1, the PDFs of q_c differences (model
436 – observation) are plotted in Figures 5a and 5b for 60-km and 180-km equivalent sizes. Figure
437 5c shows the average percentages of model q_c adjustments for different equivalent sizes. The
438 mode and average values for the 30-km equivalent size is negative, suggesting that models
439 need to simulate lower q_c in general to get reasonable autoconversion rates. Lower q_c values
440 are usually associated with smaller E_{auto} values that induce lower simulated precipitation
441 frequency. On average, the percentage of q_c adjustments decreasess with increasing equivalent
442 size. For example, the adjustments for finer resolutions (e.g., 30-60 km) can be ~20% of the q_c ,
443 whereas adjustments in coarse resolution models (e.g., 120 – 180 km) are relatively small
444 because the prescribed E_{auto} (=3.2) is close to the observed ones (Figure 4),z and when equivalent
445 size is 180-km, no adjustment is needed. The adjustment method presented in Figure 5,
446 however, may change cloud water substantially and may cause a variety of subsequent issues,
447 such as altering cloud radiative effects and disrupting the hydrological cycle. The assessment
448 in Figure 5 only provides a reference to the equivalent effect on cloud water by using the
449 prescribed E_{auto} value as compared to those from observations.

450 All above discussions are based on the prescribed E_{auto} and E_{accr} values (3.2 and 1.07) in
451 MG08. ~~W~~whereas there are quite a few parameterizations that have been published so far. In
452 this study, we list E_{auto} and E_{accr} for three other widely used parameterization schemes in Table
453 3, which are given only for 60-km and 180-km equivalent sizes. The values of the exponent in
454 each scheme directly affect the values of the enhancement factors. For example, the scheme in
455 Beheng (1994) has the highest degree of nonlinearity and hence has the largest enhancement
456 factors. The scheme in Liu and Daum (2004) is very similar to the scheme in Khairoutdinov
457 and Kogan (2000) because both schemes have a physically realistic dependence on cloud water
458 content and number concentration (Wood, 2005b). For a detailed overview and discussion of
459 various existing parameterizations, please refer to Liu and Daum (2004), Liu et al. (2006a), Liu
460 et al. (2004b), Wood (2005b) and Michibata and Takemura (2015). A physical based
461 autoconversion parameterization was developed by Lee and Baik (2017) in which the scheme
462 was derived by solving the stochastic collection equation with an approximated collection
463 kernel that is constructed using the terminal velocity of cloud droplets and the collision
464 efficiency obtained from a particle trajectory model. Due to the greatly increased complexity
465 of their equation, we do not attempt to calculate E_{auto} here but it should be examined in future
466 studies due to the ~~physies feasibility~~physically appealing of the Lee and Baik (2017) scheme.
467

468 **5. Summary**

469 To better understand the influence of sub-grid cloud variations on the warm-rain process
470 simulations in GCMs, we investigated the warm-rain parameterizations of autoconversion
471 (E_{auto}) and accretion (E_{accr}) enhancement factors in MG08. These two factors represent the
472 effects of sub-grid cloud and precipitation variabilities when parameterizing autoconversion
473 and accretion rates as functions of grid-mean quantities. E_{auto} and E_{accr} are prescribed as 3.2
474 and 1.07, respectively, in the widely used MG08 scheme. To assess the dependence of the two
475 parameters on sub-grid scale variabilities, we used ground-based observations and retrievals
476 collected at the DOE ARM Azores site to reconstruct the two enhancement factors in different
477 equivalent sizes.

478 From the retrieved q_c and q_r profiles, the averaged q_c within the top five range gates are
479 used to calculate E_{auto} and the averaged q_c and q_r within five range gates around maximum
480 reflectivity are used to calculate E_{accr} . The calculated E_{auto} values from observations and
481 retrievals increase from 1.96 at an equivalent size of 30 km to 3.18 at an equivalent size of 150
482 km. These values are 38% and 0.625% lower than the prescribed value of 3.2. The prescribed
483 value in MG08 represents well ~~in~~the large grid sizes in GCMs (e.g., 180^2 km² grid). On the
484 other hand, the E_{accr} values increase from 1.53 at an equivalent size of 30 km to 1.76 at an
485 equivalent size of 180 km, which are 43% and 64% higher than the prescribed value (1.07).
486 The higher E_{auto} and lower E_{accr} prescribed in GCMs help to explain the issue of too frequent

487 precipitation events with too light precipitation intensity. The ratios of rain to cloud liquid water
488 increase with increasing E_{accr} from 0 to 2, and then decrease ~~after that thereafter, suggesting a~~
489 ~~possible optimal state for the collision-coalescence process to achieve maximum efficiency for~~
490 ~~converting cloud water into rain water at $E_{accr}=2$. The ratios of q_r to q_e and the values~~ at
491 $E_{accr}=1.07$ and $E_{accr}=2.0$ are 0.063 and 0.142, further ~~proving underscoring~~ that the prescribed
492 value of $E_{accr}=1.07$ is too small to simulate correct precipitation intensity in models.

493 To further investigate what conditions and parameters can significantly influence the
494 enhancement factors, we classified low-level clouds according to their boundary layer
495 conditions and CLWPs. Both E_{auto} and E_{accr} increase when the boundary layer conditions
496 become less stable, and the values are larger in precipitating clouds ($CLWP > 75 \text{ gm}^{-2}$) than
497 those in nonprecipitating clouds ($CLWP < 75 \text{ gm}^{-2}$). The E_{auto} values in both stable and mid-stable
498 boundary layer conditions are smaller than the prescribed value of 3.2, while those in unstable
499 boundary layers conditions are significantly larger than 3.2 regardless of whether or not the
500 cloud is precipitating (Table 2). All E_{accr} values are greater than the prescribed value of 1.07.
501 Therefore, the selection of E_{auto} and E_{accr} values in GCMs should be regime-dependent, which
502 also has been suggested by Hill et al. (2015) and Walters et al. (2017).

503 This study, however, did not include the effect of uncertainties in GCM simulated cloud
504 and precipitation properties on sub-grid scale variations. For example, we did not consider the
505 behavior of the two enhancement factors under different aerosol regimes, a condition which

506 may affect the precipitation formation process. The effect of aerosol-cloud-precipitation-
507 interactions on cloud and precipitation sub-grid variabilities may be of comparable importance
508 to meteorological regimes and precipitation status and deserves a further study. Other than the
509 large-scale dynamics, e.g., LTS in this study, upward/downward motion in sub-grid scale may
510 also modify cloud and precipitation development and affect the calculations of enhancement
511 factors. The investigation of the dependence of E_{auto} and E_{accr} on aerosol type and concentration
512 as well as on vertical velocity would be a natural extension and complement of the current
513 study. In addition, other factors may also affect precipitation frequency and intensity even
514 under the same aerosol regimes and even if the clouds have similar cloud water contents. Wind
515 shear, for example as presented in Wu et al. (2017), is an external variable that can affect
516 precipitation formation. Further studies are needed to evaluate the role of the covariance of q_c
517 and N_c ~~in-at~~ sub-grid scales on E_{auto} ~~determinations~~, which is beyond the scope of this study
518 and requires independent retrieval techniques.

519

520 **Appendix A: Joint cloud and rain LWC profile estimation**

521 If a time step is identified as non-precipitating, the cloud liquid water content (CLWC)
522 profile is retrieved using Frisch et al. (1995) and Dong et al. (1998, 2014a and 2014b). The
523 retrieved CLWC is proportional to radar reflectivity.

524 If a time step is identified as precipitating (maximum reflectivity below cloud base
 525 exceeds -37 dBZ), CLWC profile is first inferred from temperature and pressure in merged
 526 sounding by assuming adiabatic growth. Marine stratocumulus clouds isare close to adiabatic
 527 (Albrecht et al. 1990) ~~and was used in cloud property retrievals in literature~~ which assists cloud
 528 property retrievals (e.g., Rémillard et al., 2013). In this study, we use the information from rain
 529 properties near cloud base to further constrain the adiabatic CLWC ($CLWC_{adiabatic}$).

530 Adopting the method of O'Connor et al. (2005), Wu et al. (2015) retrieved rain properties
 531 below cloud base (CB) for the same period as in this study. In Wu et al. (2015), rain drop size
 532 (median diameter, D_0), shape parameter (μ), and normalized rain droplet number concentration
 533 (N_W) are retrieved for the assumed rain particle size distribution (PSD):

$$534 \quad n_r(D) = N_W f(\mu) \left(\frac{D}{D_0}\right)^\mu \exp\left[-\frac{(3.67+\mu)D}{D_0}\right] \quad (A1)$$

535 To infer rain properties above cloud base, we adopt the assumption in Fielding et al. (2015)
 536 that N_W increases from below CB to within the cloud. This assumption is consistent with the *in*
 537 *situ* measurement in Wood (2005a). Similar ~~as to~~ Fielding et al. (2015), we use constant N_W
 538 within cloud if the vertical gradient of N_W is negative below CB. The μ within cloud is treated
 539 as constant and is taken as the average value from four range gates below CB. Another
 540 assumption in the retrieval is that the evaporation of rain drops is negligible from one range
 541 gate above CB to one range gate below CB thus we assume rain drop size is the same at the
 542 range gate below and above CB.

543 With the above information, we can calculate the reflectivity contributed by rain at the first
 544 range gate above CB ($Z_r(1)$) and the cloud reflectivity ($Z_c(1)$) is then $Z_c(1) = Z(1) - Z_r(1)$,
 545 where $Z(1)$ is the WACR measured reflectivity at the first range gate above CB. Using the
 546 cloud droplet number concentration (N_c) from Dong et al. (2014a and 2014b), CLWC at the
 547 first range gate above CB can be calculated through

$$548 \quad Z_c(1) = 2^6 \int_0^\infty n_c(r) r^6 dr = \frac{36}{\pi^2 \rho_w^2} \frac{CLWC(1)_{reflectivity}^2}{N_c} \exp(9\sigma_x^2) \quad (A2.1)$$

$$549 \quad CLWC(1)_{reflectivity} = \sqrt{\frac{Z_c(1) \pi^2 \rho_w^2 N_c}{36 \exp(9\sigma_x^2)}} \quad (A2.2)$$

550 Where ρ_w is liquid water density $n_c(r)$ is lognormal distribution of cloud PSD with
 551 logarithmic width σ_x . Geoffroy et al. (2010) suggested that σ_x increases with the length scale
 552 and Witte et al. (2018) showed that σ_x is also dependent on the choice of instrumentation. The
 553 variations of σ_x should be reflected in the retrieval by using different σ_x values with time.
 554 However, no aircraft measurements were available during CAP-MBL to provide σ_x over the
 555 Azores region. The inclusion of solving σ_x in the retrieval adds another degree of freedom to
 556 the equations and complicates the problem considerably. In this study, σ_x is set to a constant
 557 value of 0.38 from Miles et al. (2000), which is a statistical value from aircraft measurements
 558 inef marine low-level clouds.

559 We then compare the $CLWC_{adiabatic}$ and the one calculated from $CLWC_{reflectivity}$ at the
 560 first range gate above CB. A scale parameter (s) is defined as $s = \frac{CLWC_{reflectivity}(1)}{CLWC_{adiabatic}(1)}$ and the

561 entire profile of $CLWC_{adiabatic}$ is multiplied by s to correct the bias from cloud sub-
562 adiabaticity. ~~The R~~reflectivity profile from the cloud is then calculated from Eq. (A2.1) using
563 the updated $CLWC_{adiabatic}$ and the remaining reflectivity profile from the WACR observation
564 is regarded as the rain contribution. Rain particle size can then be calculated given that N_W and
565 μ are known and rain liquid water content (RLWC) can be estimated.

566 There are two constrains used in the retrieval. One is that the summation of cloud and rain
567 liquid water path (CLWP and RLWP) must be equal to the LWP from the microwave
568 radiometer observation. Another is that rain drop size (D_0) near cloud top muyst be equal or
569 greater than $50 \mu m$ and if D_0 is less than $50 \mu m$, we decrease N_W for the entire rain profile
570 within cloud and repeat the calculation until the $50 \mu m$ criteriona is satisfied.

571 It is difficult to quantitatively estimate the retrieval uncertainties without aircraft in situ
572 measurements. For the proposed retrieval method, 18% should be used as uncertainty for
573 RLWC from rain properties in Wu et al. (2015) and 30% for CLWC from cloud properties in
574 Dong et al. (2014a and 2014b). The actual uncertainty depends on the accuracy of the merged
575 sounding data, the ~~detectability~~sensitivity of WACR near cloud base and the effect of
576 entrainment on cloud adiabaticity during precipitating. ~~In the~~A recent aircraft field campaign,
577 the Aerosol and Cloud Experiments in Eastern North Atlantic (ACE-ENA), was conducted
578 during 2017-2018 with a total of 39 flights over the Azores, near the ARM ENA site on

579 Graciosa Island. These aircraft in situ measurements will be used to validate the ground-based
580 retrievals and quantitatively estimate their uncertainties in the future.

581 Figure A1 shows an example of the retrieval results. The merged sounding, ceilometer,
582 microwave radiometer, WACR and ceilometer are used in the retrieval. Whenever one or more
583 instruments are not reliable, that time step is skipped, and this results in the gaps in the CLWC
584 and RLWC as shown in Figures A1(b) and A1(c). When the cloud is classified as
585 nonprecipitating, no RLWC will be retrieved ~~as well~~. Using air density (ρ_{air}) profiles
586 calculated from temperature and pressure in merged sounding, mixing ratio (q) can be
587 calculated from LWC using $q(z) = LWC(z)/\rho_{air}(z)$.

588 **Acknowledgements**

589 The ground-based measurements were obtained from the Atmospheric Radiation Measurement
590 (ARM) Program sponsored by the U.S. Department of Energy (DOE) Office of Energy
591 Research, Office of Health and Environmental Research, and Environmental Sciences
592 Division. The data can be downloaded from <http://www.archive.arm.gov/>. This research was
593 supported by the DOE CESM project under grant DE-SC0014641 at the University of Arizona
594 through subaward from University of Maryland at Baltimore County, and the NSF project
595 under grant AGS-1700728 at University of Arizona. The authors thank Dr. Yangang Liu at
596 Brookhaven National Laboratory for insightful comments and Ms. Casey E. Oswant at the

597 University of Arizona for proof reading the manuscript. The three anonymous reviewers are
598 acknowledged for constructive comments and suggestions, which helped to improve the
599 manuscript. We appreciate the comments and corrections from the CO Editor, Dr. Graham
600 Feingold.

601

602 **References**

603 Ahlgrim, M., and Forbes, R.: Improving the Representation of Low Clouds and Drizzle in
604 the ECMWF Model Based on ARM Observations from the Azores, *J. Clim.*, doi:
605 10.1175/MWR-D-13-00153.1, 2014.

606 Albrecht, B., Fairall, C., Thomson, D., White, A., Snider, J., and Schubert, W.: Surface-based
607 remote-sensing of the observed and the adiabatic liquid water-content of stratocumulus
608 clouds, *Geophys. Res. Lett.*, 17, 89–92, doi:10.1029/G1017i001p00089, 1990.

609 Austin, P., Wang, Y., Kujala, V., and Pincus, R.: Precipitation in Stratocumulus Clouds:
610 Observational and Modeling Results, *J. Atmos. Sci.*, 52, 2329–2352, doi:10.1175/1520-
611 0469(1995)052<2329:PISCOA>2.0.CO;2, 1995.

612 Bai, H., Gong, C., Wang, M., Zhang, Z., and L'Ecuyer, T.: Estimating precipitation
613 susceptibility in warm marine clouds using multi-sensor aerosol and cloud products from
614 A-Train satellites, *Atmos. Chem. Phys.*, 18, 1763-1783, [https://doi.org/10.5194/acp-18-](https://doi.org/10.5194/acp-18-1763-2018)
615 [1763-2018](https://doi.org/10.5194/acp-18-1763-2018), 2018.

616 Barker H. W., Wiellicki B.A., Parker L.: A parameterization for computing grid-averaged solar
617 fluxes for inhomogeneous marine boundary layer clouds. Part II: Validation using satellite
618 data. *J. Atmos. Sci.* 53: 2304–2316, 1996.

619 Beheng, K. D.: A parameterization of warm cloud microphysical conversion processes, *Atmos.*
620 *Res.*, 33, 193-206, 1994.

621 Bony, S., and Dufresne, J.-L.: Marine boundary layer clouds at the heart of tropical cloud
622 feedback uncertainties in climate models, *Geophys. Res. Lett.*, 32, L20806,
623 doi:10.1029/2005GL023851, 2005.

624 Boutle, I. A., Abel, S. J., Hill, P. G., and Morcrette, C. J.: Spatial variability of liquid cloud and
625 rain: Observations and microphysical effects. *Quart. J. Roy. Meteor. Soc.*, 140, 583–594,
626 doi:10.1002/qj.2140, 2014.

627 Chen, T., Rossow, W. B., and Zhang, Y.: Radiative Effects of Cloud-Type Variations, *J. Clim.*,
628 13, 264–286, 2000.

629 Cheng, A., and Xu. K.-M.: A PDF-based microphysics parameterization for simulation of
630 drizzling boundary layer clouds, *J. Atmos. Sci.*, 66, 2317–2334,
631 doi:10.1175/2009JAS2944.1, 2009.

632 Comstock, K. K., Yuter, S. E., Wood, R., and Bretherton, C. S.: The Three-Dimensional
633 Structure and Kinematics of Drizzling Stratocumulus, *Mon. Weather Rev.*, 135, 3767–
634 3784, doi:10.1175/2007MWR1944.1, 2007.

635 Dong X., Ackerman, T. P., and Clothiaux, E. E.: Parameterizations of Microphysical and
636 Radiative Properties of Boundary Layer Stratus from Ground-based measurements, *J.*
637 *Geophys. Res.*, 102, 31,681-31,393, 1998.

638 Dong, X., Minnis, P., Ackerman, T. P., Clothiaux, E. E., Mace, G. G., Long, C. N., and
639 Liljegren, J. C.: A 25-month database of stratus cloud properties generated from ground-
640 based measurements at the ARM SGP site, *J. Geophys. Res.*, 105, 4529-4538, 2000.

641 Dong, X., Xi, B., Kennedy, A., Minnis, P. and Wood, R.: A 19-month Marine Aerosol-
642 Cloud_Radiation Properties derived from DOE ARM AMF deployment at the Azores:
643 Part I: Cloud Fraction and Single-layered MBL cloud Properties, *J. Clim.*, 27,
644 doi:10.1175/JCLI-D-13-00553.1, 2014a.

645 Dong, X., Xi, B., and Wu, P.: Investigation of Diurnal Variation of MBL Cloud Microphysical
646 Properties at the Azores, *J. Clim.*, 27, 8827-8835, 2014b.

647 Fielding, M. D., Chiu, J. C., Hogan, R. J., Feingold, G., Eloranta, E., O'Connor, E. J. and
648 Cadeddu, M. P.: Joint retrievals of cloud and drizzle in marine boundary layer clouds using
649 ground-based radar, lidar and zenith radiances. *Atmospheric Measurement Techniques*, 8,
650 pp. 2663-2683. ISSN 1867-8548 doi: 10.5194/amt-8-2663-2015, 2015.

651 Frisch, A., Fairall, C., and Snider, J.: Measurement of stratus cloud and drizzle parameters in
652 ASTEX with a Ka-band Doppler radar and a microwave radiometer, *J. Atmos. Sci.*, 52,
653 2788–2799, 1995.

654 Geoffroy, O., Brenguier, J.-L., and Burnet, F.: Parametric representation of the cloud droplet
655 spectra for LES warm bulk microphysical schemes, *Atmos. Chem. Phys.*, 10, 4835-4848,
656 <https://doi.org/10.5194/acp-10-4835-2010>, 2010.

657 Hahn, C. and Warren, S.: A gridded climatology of clouds over land (1971–96) and ocean
658 (1954–97) from surface observations worldwide, Numeric Data Package NDP-026E
659 ORNL/CDIAC-153, CDIAC, Department of Energy, Oak Ridge, Tennessee, 2007.

660 Hartmann, D. L., Ockert-Bell, M. E., and Michelsen, M. L.: The Effect of Cloud Type on
661 Earth's Energy Balance: Global Analysis, *J. Climate*, 5, 1281–1304,
662 [https://doi.org/10.1175/15200442\(1992\)005<1281:TEOCTO>2.0.CO;2](https://doi.org/10.1175/15200442(1992)005<1281:TEOCTO>2.0.CO;2), 1992.

663 Hartmann, D. L. and Short, D. A.: On the use of earth radiation budget statistics for studies of
664 clouds and climate, *J. Atmos. Sci.*, 37, 1233–1250, doi:10.1175/1520-
665 0469(1980)037<1233:OTUOER>2.0.CO;2, 1980.

666 Hill, P. G., Morcrette, C. J., and Boutle, I. A.: A regime-dependent parametrization of subgrid-
667 scale cloud water content variability, *Q. J. R. Meteorol. Soc.*, 141, 1975–1986, 2015.

668 Houghton, J. T., Ding, Y., Griggs, D.J., Noguer, M., van der Linden, P.J., Dai, X., Maskell, K.,
669 and Johnson, C.A.: *Climate Change: The Scientific Basis*, Cambridge University Press,
670 881 pp, 2001.

671 Jess, S.: Impact of subgrid variability on large-scale precipitation formation in the climate
672 model ECHAM5, PhD thesis, Dep. of Environ. Syst. Sci., ETH Zurich, Zurich,
673 Switzerland, 2010.

674 Jiang, J., Su, H., Zhai, C., Perun, V. S., Del Genio, A., Nazarenko, L. S., Donner, L. J.,
675 Horowitz, Seman, L., Cole, C., J., Gettelman, A., Ringer, M. A., Rotstayn, L., Jeffrey, S.,
676 Wu, T., Brient, F., Dufresne, J-L., Kawai, H., Koshiro, T., Watanabe, M., LÉcuyer, T. S.,
677 Volodin, E. M., Iversen, Drange, T., H., Mesquita, M. D. S., Read, W. G., Waters, J. W.,
678 Tian, B., Teixeira, J., and Stephens, G. L.: Evaluation of cloud and water vapor simulations
679 in CMIP5 climate models using NASA “A-train” satellite observations, *J. Geophys. Res.*,
680 117, D14105, doi:10.1029/2011JD017237, 2012.

681 Kessler, E.: On the distribution and continuity of water substance in atmospheric circulations,
682 *Met. Monograph* 10, No. 32, American Meteorological Society, Boston, USA, 84 pp.,
683 1969.

684 Khairoutdinov, M. and Kogan, Y.: A New Cloud Physics Parameterization in a Large-Eddy
685 Simulation Model of Marine Stratocumulus, *Mon. Wea. Rev.*, 128, 229-243, 2000.

686 Kollias, P., Szyrmer, W., Rémillard, J., and Luke, E.: Cloud radar Doppler spectra in drizzling
687 stratiform clouds:2. Observations and microphysical modeling of drizzle evolution, *J.*
688 *Geophys. Res.*, 116, D13203, doi:10.1029/2010JD015238, 2011.

689 Kooperman, G. J., Pritchard, M. S., Ghan, S. J., Wang, M., Somerville, R. C., and Russell, L.
690 M.: Constraining the influence of natural variability to improve estimates of global aerosol
691 indirect effects in a nudged version of the Community Atmosphere Model 5, *J. Geophys.*
692 *Res.*, 117, D23204, <https://doi.org/10.1029/2012JD018588>, 2012.

693 Kubar, T. L., Hartmann, D. L., and Wood, R.: Understanding the importance of microphysics
694 and macrophysics in marine low clouds, Part I: satellite observations. *J. Atmos. Sci.*, 66,
695 2953-2972, doi: 10.1175/2009JAS3071.1, 2009.

696 Larson, V. E., Nielsen, B. J., Fan, J., and Ovchinnikov, M.: Parameterizing correlations
697 between hydrometeor species in mixed-phase Arctic clouds, *J. Geophys. Res.*, 116,
698 D00T02, doi:10.1029/2010JD015570, 2011.

699 Larson, V. E., and Griffin, B. M.: Analytic upscaling of a local microphysics scheme. Part I:
700 Derivation. *Quart. J. Roy. Meteor. Soc.*, 139, 46–57, 2013.

701 Lebsock, M. D., Morrison, H., and Gettelman, A.: Microphysical implications of cloud-
702 precipitation covariance derived from satellite remote sensing, *J. Geophys. Res.-Atmos.*,
703 118, 6521–6533, <https://doi.org/10.1002/jgrd.50347>, 2013.

704 Lee, H., and Baik, J.-J.: A physically based autoconversion parameterization. *Journal of the*
705 *Atmospheric Sciences*, 74, 1599–1616, 2017.

706 Leon, D. C., Wang, Z., and Liu, D.: Climatology of drizzle in marine boundary layer clouds
707 based on 1 year of data from CloudSat and Cloud-Aerosol Lidar and Infrared Pathfinder
708 Satellite Observations (CALIPSO), *J. Geophys. Res.*, 113, D00A14,
709 doi:10.1029/2008JD009835, 2008.

710 Liljegren, J. C., Clothiaux, E. E., Mace, G. G., Kato, S., and Dong, X.: A new retrieval for
711 cloud liquid water path using a ground-based microwave radiometer and measurements of
712 cloud temperature, *J. Geophys. Res.*, 106, 14,485–14,500, 2001.

713 Liu, Y. and Daum, P. H.: Parameterization of the autoconversion process, Part I: Analytical
714 formulation of the Kessler-type parameterizations, *J. Atmos. Sci.*, 61, 1539–1548, 2004.

715 Liu, Y., Daum, P. H., and McGraw, R.: Parameterization of the autoconversion process. Part
716 II: Generalization of Sundqvist-type parameterizations, *J. Atmos. Sci.*, 63, 1103–1109,
717 2006a.

718 Liu, Y., Daum, P. H., McGraw, R., Miller, M.: Generalized threshold function accounting for
719 effect of relative dispersion on threshold behavior of autoconversion process. *Geophys.*
720 *Res. Lett.*, 33, L11804, 2006b.

721 Michibata, T., and Takemura, T.: Evaluation of autoconversion schemes in a single model
722 framework with satellite observations, *J. Geophys. Res. Atmos.*, 120, 9570–9590,
723 doi:10.1002/2015JD023818, 2015.

724 Miles, N. L., Verlinde, J., and Clothiaux, E. E.: Cloud-droplet size distributions in low-level
725 stratiform clouds. *J. Atmos. Sci.*, 57, 295–311, doi:10.1175/1520-0469(2000)057,
726 0295:CDS DIL.2.0.CO;2, 2000.

727 Morrison, H. and Gettelman, A.: A new two-moment bulk stratiform cloud microphysics
728 scheme in the Community Atmosphere Model, version 3 (CAM3). Part I: Description and
729 numerical tests, *J. Climate*, 21, 3642–3659, 2008.

730 Nam, C., and Quaas, J.: Evaluation of clouds and precipitation in the ECHAM5 general
731 circulation model using CALIPSO and CloudSat satellite data, *J. Clim.*, 25, 4975–4992,
732 doi:10.1175/JCLI-D-11-00347.1, 2012.

733 O’Connor, E. J., Hogan, R. J., and Illingworth, A. J.: Retrieving stratocumulus drizzle
734 parameters using Doppler radar and lidar, *J. of Applied Meteorol.*, 44, 14-27, 2005.

735 Platnick, S. and Twomey, S.: Determining the Susceptibility of Cloud Albedo to Changes in
736 Droplet Concentration with the Advanced Very High Resolution Radiometer, *J. Appl.*
737 *Meteorol.*, 33, 334–347, 1994.

738 Pincus, R., McFarlane, S. A., and Klein, S. A.: Albedo bias and the horizontal variability of
739 clouds in subtropical marine boundary layers: Observations from ships and satellites, *J.*
740 *Geophys. Res.*, 104, 6183–6191, doi:10.1029/1998JD200125, 1999.

741 Pincus, R., and Klein, S. A.: Unresolved spatial variability and microphysical process rates in
742 large-scale models. *J. Geophys. Res.*, 105D, 27 059–27 065, 2000.

743 ~~Quaas, J., Ming, Y., Menon, S., Takemura, T., Wang, M., Penner, J. E., Gettelman, A.,~~
744 ~~Lohmann, U., Bellouin, N., Boucher, O., Sayer, A. M., Thomas, G. E., McComiskey, A.,~~
745 ~~Feingold, G., Hoose, C., Kristjánsson, J. E., Liu, X., Balkanski, Y., Donner, L. J., Ginoux,~~
746 ~~P. A., Stier, P., Grandey, B., Feichter, J., Sednev, Bauer, S. E., Koch, D., Grainger, R. G.,~~

747 ~~Kirkevåg, A., Iversen, T., Seland, Ø., Easter, R., Ghan, S. J., Rasch, P. J., Morrison, H.,~~
748 ~~Lamarque, J. F., Iacono, M. J., Kinne, S., and Schulz, M.: Aerosol indirect effects—~~
749 ~~general circulation model intercomparison and evaluation with satellite data, Atmos.~~
750 ~~Chem. Phys., 9, 8697–8717, <https://doi.org/10.5194/acp-9-8697-2009>, 2009.~~

751 Randall, D. A., Coakley, J. A., Fairall, C. W., Knopfli, R. A., and Lenschow, D. H.: Outlook
752 for research on marine subtropical stratocumulus clouds. Bull. Amer. Meteor. Soc., 65,
753 1290–1301, 1984.

754 Rémillard, J., Kollias, P., Luke, E., and Wood, R.: Marine Boundary Layer Cloud Observations
755 in the Azores, J. Climate, 25, 7381–7398, doi: [http://dx.doi.org/10.1175/JCLI-D-11-](http://dx.doi.org/10.1175/JCLI-D-11-00610.1)
756 [00610.1](http://dx.doi.org/10.1175/JCLI-D-11-00610.1), 2012.

757 Rémillard, J., Kollias, P., and Szyrmer, W.: Radar-radiometer re-
758 trievals of cloud number concentration and dispersion parameter in nondrizzling marine stratocumulus, Atmos.
759 Meas. Tech., 6, 1817–1828, doi:10.5194/amt-6-1817-2013, 2013.

760 Sauvageot, H., and Omar, J.: Radar reflectivity of cumulus clouds, J. Atmos. Oceanic Technol.,
761 4, 264–272, 1987.

762 Slingo, A.: Sensitivity of the Earth’s radiation budget to changes in low clouds, Nature, 343,
763 49–51, <https://doi.org/10.1038/343049a0>, 1990.

764 Song, H., Zhang, Z., Ma, P.-L., Ghan, S. J., and Wang, M.: An Evaluation of Marine Boundary
765 Layer Cloud Property Simulations in the Community Atmosphere Model Using Satellite
766 Observations: Conventional Subgrid Parameterization versus CLUBB, J. Clim.,
767 doi:10.1175/JCLI-D-17-0277.1, 2018.

768 Stanfield, R., Dong, X., Xi, B., Gel Genio, A., Minnis, P., and Jiang, J.: Assessment of NASA
769 GISS CMIP5 and post CMIP5 Simulated Clouds and TOA Radiation Budgets Using
770 Satellite Observations: Part I: Cloud Fraction and Properties, J. Clim., doi:10.1175/JCLI-
771 D-13-00588.1, 2014.

772 Tripoli, G. J. and Cotton, W. R.: A numerical investigation of several factors contributing to
773 the observed variable intensity of deep convection over South Florida., *J. Appl. Meteorol.*,
774 19, 1037–1063, 1980.

775 Troyan, D.: Merged Sounding Value-Added Product, Tech. Rep., DOE/SC-ARM/TR-087,
776 2012.

777 Walters, D., Baran, A., Boutle, I., Brooks, M., Earnshaw, P., Edwards, J., Furtado, K., Hill, P.,
778 Lock, A., Manners, J., Morcrette, C., Mulcahy, J., Sanchez, C., Smith, C., Stratton, R.,
779 Tennant, W., Tomassini, L., van Weverberg, K., Vosper, S., Willett, M., Browse, J.,
780 Bushell, A., Dalvi, M., Essery, R., Gedney, N., Hardiman, S., Johnson, B., Johnson, C.,
781 Jones, A., Mann, G., Milton, S., Rumbold, H., Sellar, A., Ujiie, M., Whittall, M., Williams,
782 K. and Zerroukat, M. The Met Office Unified Model Global Atmosphere 7.0/7.1 and
783 JULES Global Land 7.0 configurations. *Geosci. Model Dev.*, doi:10.5194/gmd-2017-291,
784 2017.

785 Wang, J., and Geerts, B.: Identifying drizzle within marine stratus with W-band radar
786 reflectivity, *Atmos. Res.*, 69, 1–27, 2003.

787 Wang, M., Ghan, S., Liu, X., L’Ecuyer, T. S., Zhang, K., Morrison, H., Ovchinnikov, M.,
788 Easter, R., Marchand, R., Chand, D., Qian, Y., and Penner, J. E.: Constraining cloud
789 lifetime effects of aerosols using A-Train satellite observations, *Geophys. Res. Lett.*, 39,
790 L15709, <https://doi.org/10.1029/2012GL052204>, 2012.

791 Warren, S. G., Hahn, C. J., London, J., Chervin, R. M., and Jenne, R.: Global distribution of
792 total cloud cover and cloud type amount over land, Tech. Rep. Tech. Note TN-317 STR,
793 NCAR, 1986.

794 Warren, S. G., Hahn, C. J., London, J., Chervin, R. M., and Jenne, R.: Global distribution of
795 total cloud cover and cloud type amount over land, Tech. Rep. Tech. Note TN-317 STR,
796 NCAR, 1988.

797 Weber, T., and Quaas, J.: Incorporating the subgrid-scale variability of clouds in the
798 autoconversion parameterization using a PDF-scheme, *J. Adv. Model. Earth Syst.*, 4,
799 M11003, doi:10.1029/2012MS000156, 2012.

800 Wielicki, B. A., Cess, R. D., King, M. D., Randall, D. A., and Harrison, E. F.: Mission to planet
801 Earth: Role of clouds and radiation in climate, *Bull. Amer. Meteor. Soc.*, 76, 2125–2153,
802 doi:10.1175/1520-0477(1995)076<2125:MTPERO.2.0.CO;2, 1995.

803 Witte, M. K., Yuan, T., Chuang, P. Y., Platnick, S., Meyer, K. G., Wind, G., and Jonsson, H.
804 H.: MODIS retrievals of cloud effective radius in marine stratocumulus exhibit no
805 significant bias. *Geophysical Research Letters*, 45, 10,656–10,664.
806 <https://doi.org/10.1029/2018GL079325>, 2018.

807 Wood, R., Field, P. R., and Cotton, W. R.: Autoconversion rate bias in stratiform boundary
808 layer cloud parameterization. *Atmos. Res.*, 65, 109–128, 2002.

809 Wood, R.: Drizzle in stratiform boundary layer clouds. Part I: Vertical and horizontal structure,
810 *J. Atmos. Sci.*, 62, 3011–3033, 2005a.

811 Wood, R.: Drizzle in stratiform boundary layer clouds. Part II: Microphysical aspects, *J.*
812 *Atmos. Sci.*, 62, 3034–3050, 2005b.

813 Wood, R. and Hartmann, D.: Spatial variability of liquid water path in marine low cloud: The
814 importance of mesoscale cellular convection, *J. Climate*, 19, 1748–1764, 2006.

815 Wood, R.: Cancellation of aerosol indirect effects in marine stratocumulus through cloud
816 thinning. *J. Atmos. Sci.*, 64, 2657–2669, 2007.

817 Wood, R.: Stratocumulus Clouds, *Mon. Wea. Rev.*, 140, 2373–2423. doi:
818 <http://dx.doi.org/10.1175/MWR-D-11-00121.1>, 2012.

819 Wood, R., Wyant, M., Bretherton, C. S., Rémillard, J., Kollias, P., Fletcher, J., Stemmler, J.,
820 deSzoeko, S., Yuter, S., Miller, M., Mechem, D., Tselioudis, G., Chiu, C., Mann, J.,
821 O'Connor, E., Hogan, R., Dong, X., Miller, M., Ghate, V., Jefferson, A., Min, Q., Minnis,
822 P., Palinkonda, R., Albrecht, B., Luke, E., Hannay, C., Lin, Y.: Clouds, Aerosol, and

823 Precipitation in the Marine Boundary Layer: An ARM Mobile Facility Deployment, Bull.
824 Amer. Meteorol. Soc., doi: <http://dx.doi.org/10.1175/BAMS-D-13-00180.1>, 2015.

825 Wu, P., Dong, X. and Xi, B.: Marine boundary layer drizzle properties and their impact on
826 cloud property retrieval, *Atmos. Meas. Tech.*, 8, 3555–3562. doi: 10.5194/amt-8-3555-
827 2015, 2015.

828 Wu, P., Dong, X., Xi, B., Liu, Y., Thieman, M., and Minnis, P.: Effects of environment forcing
829 on marine boundary layer cloud-drizzle processes, *J. Geophys. Res. Atmos.*, 122, 4463–
830 4478, doi:10.1002/2016JD026326, 2017.

831 Xie, X., and Zhang, M.: Scale-aware parameterization of liquid cloud inhomogeneity and its
832 impact on simulated climate in CESM, *J. Geophys. Res. Atmos.*, 120, 8359–8371,
833 doi:10.1002/2015JD023565, 2015.

834 Yoo, H., and Li, Z.: Evaluation of cloud properties in the NOAA/NCEP Global Forecast
835 System using multiple satellite products. *Climate Dyn.*, 39, 2769–2787,
836 doi:10.1007/s00382-012-1430-0, 2012.

837 Yoo, H., and Li, Z., Hou, Y.-T., Lord, S., Weng, F., and Barker, H. W.: Diagnosis and testing
838 of low-level cloud parameterizations for the NCEP/GFS using satellite and ground-based
839 measurements. *Climate Dyn.*, 41, 1595–1613, doi:10.1007/s00382-013-1884-8, 2013.

840 Zhang, J., Lohmann, U., and Lin, B.: A new statistically based autoconversion rate
841 parameterization for use in large-scale models. *J. Geophys. Res.*, 107, 4750,
842 doi:10.1029/2001JD001484, 2002.

843 Zhang, Z., Song, H., Ma, P.-L., Larson, V., Wang, M., Dong, X., and Wang, J.: Subgrid
844 variations of cloud water and droplet number concentration over tropical oceans: satellite
845 observations and implications for warm rain simulation in climate models. Submitted to
846 *Atmos. Chem. Phys.*, 2018.

847

848 **Table 1. The parameters of autoconversion and accretion formulations for four**
 849 **parameterizations.**

850

| | A | a_1 | a_2 | B | b |
|-----------------------------------|-------------------------------------------------------------------------------------------|-------|-------|-----|------|
| Khairoutdinov and Kogan (2000) | 1350 | 2.47 | -1.79 | 67 | 1.15 |
| | $1.3 \times 10\beta_6^6$, | | | | |
| | where $\beta_6^6 = [(r_v + 3)/r_v]^2$, | | | | |
| Liu and Daum (2004) | r_v is mean volume radius. | 3 | -1 | N/A | N/A |
| | modification was made by Wood (2005b) | | | | |
| Tripoli and Cotton (1980) | 3268 | 7/3 | -1/3 | 1 | 1 |
| Beheng (1994) | 3×10^{34} for $N_c < 200 \text{ cm}^{-3}$ 9.9 for $N_c > 200 \text{ cm}^{-3}$ | 4.7 | -3.3 | 1 | 1 |

851

852 **Table 2. Autoconversion (left) and accretion (right) enhancement factors in different**
 853 **boundary layer conditions (LTS > 18 K for stable, LTS < 13.5 K for unstable and LTS**
 854 **within 13.5 and 18 K for mid-stable) and in different LWP regimes (LWP ≤ 75 g m⁻² for**
 855 **non-precipitating and LWP > 75 g m⁻² for precipitating).**

856

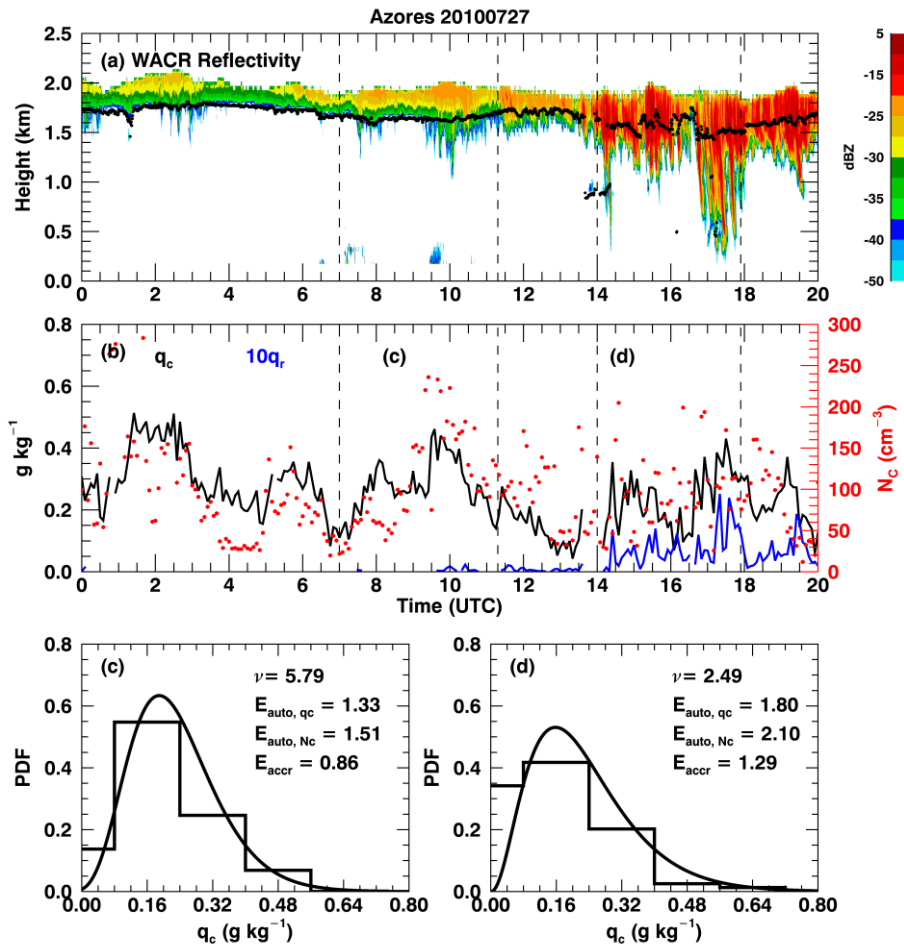
| | LWP ≤ 75 g m ⁻² | LWP > 75 g m ⁻² |
|---------------------|----------------------------|----------------------------|
| LTS > 18 K | 2.32/1.42 | 2.75/1.52 |
| 13.5 ≤ LTS ≤ 18K | 2.61/1.47 | 3.07/1.68 |
| LTS < 13.5 K | 4.62/1.72 | 6.94/1.86 |

857

858 **Table 3. Autoconversion and accretion enhancement factors (E_{auto} and E_{accr}) for the**
 859 **parameterizations in Table 1 except the Khairoutdinov and Kogan (2000) scheme. The**
 860 **values are averaged for 60-km and 180-km equivalent sizes.**
 861

| | E_{auto} | | E_{accr} | |
|------------------------------|------------|--------|------------|--------|
| | 60-km | 180-km | 60-km | 180-km |
| Liu and Daum (2004) | 3.82 | 4.23 | N/A | N/A |
| Tripoli and Cotton (1980) | 2.46 | 2.69 | 1.47 | 1.56 |
| Beheng (1994) | 6.94 | 5.88 | 1.47 | 1.56 |

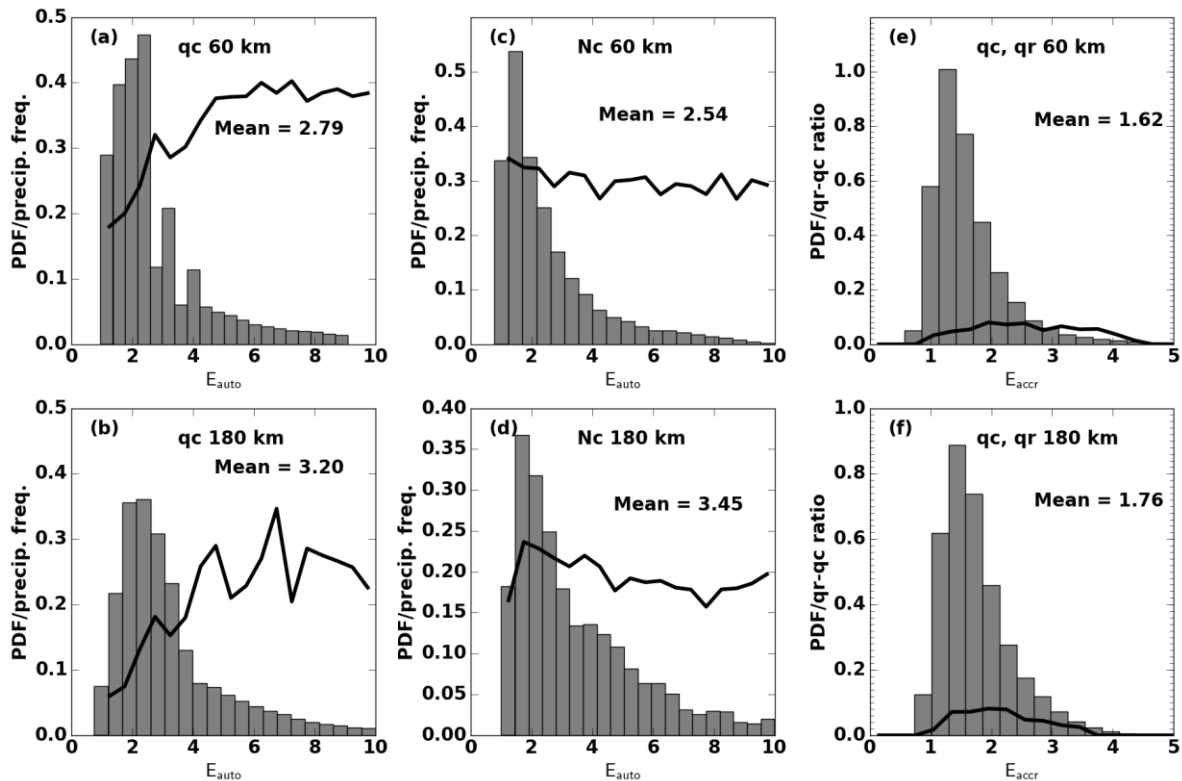
862



863

864 **Figure 1. Observations and retrievals over the Azores on 27 July 2010. (a) W-band ARM**
 865 **cloud radar (WACR) reflectivity (contour) superimposed with cloud-base height (black**
 866 **dots). (b) Black line represents averaged cloud water mixing ratio (q_c) within the top five**
 867 **range gates, blue line represents averaged rain ($\times 10$) water mixing ratio within five range**
 868 **gates around maximum reflectivity, red dots are the retrieved cloud droplet number**
 869 **concentration (N_c). Dashed lines represent two periods that have 60 km equivalent sizes**
 870 **with similar \bar{q}_c but different distributions as shown by step lines in (c) and (d). Curved**
 871 **lines in (c) and (d) are fitted gamma distributions with the corresponding shape**
 872 **parameter (ν) shown on the upper right. N_c distributions are not shown. The calculated**
 873 **autoconversion (E_{auto, q_c} from q_c and E_{auto, N_c} from N_c) and accretion (E_{accr}) enhancement**
 874 **factors are also shown.**

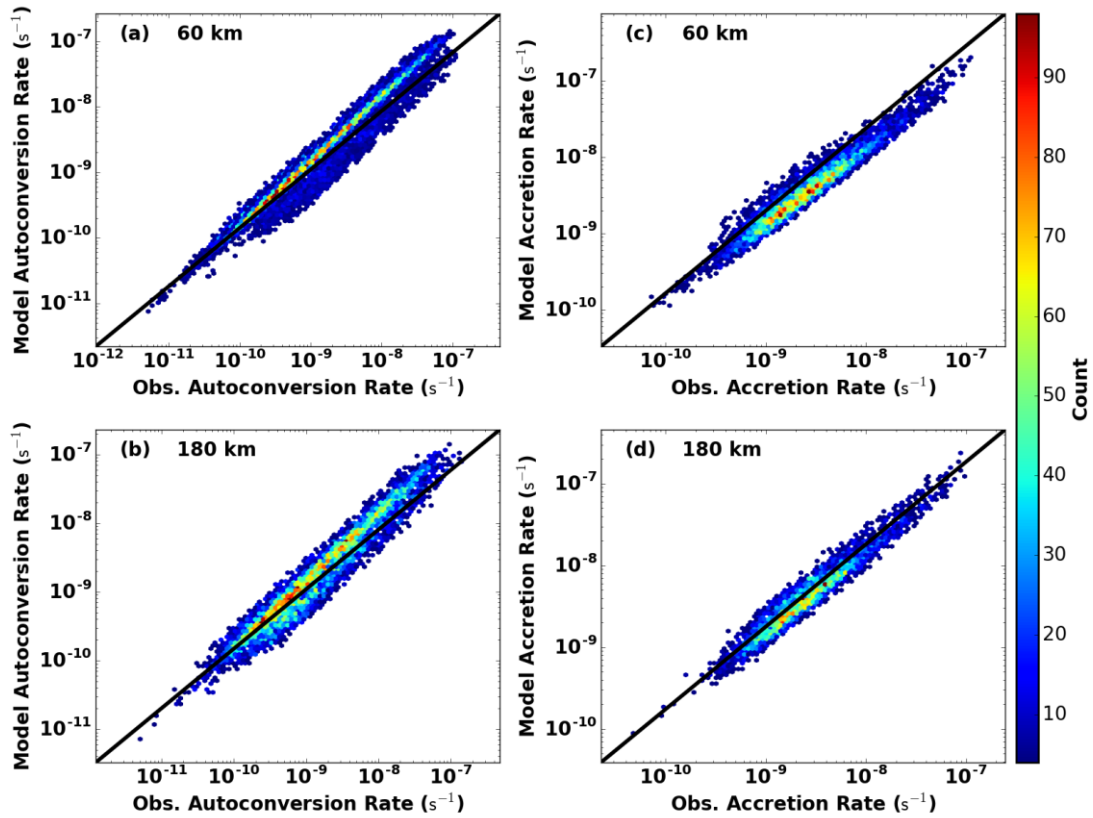
875
876



877

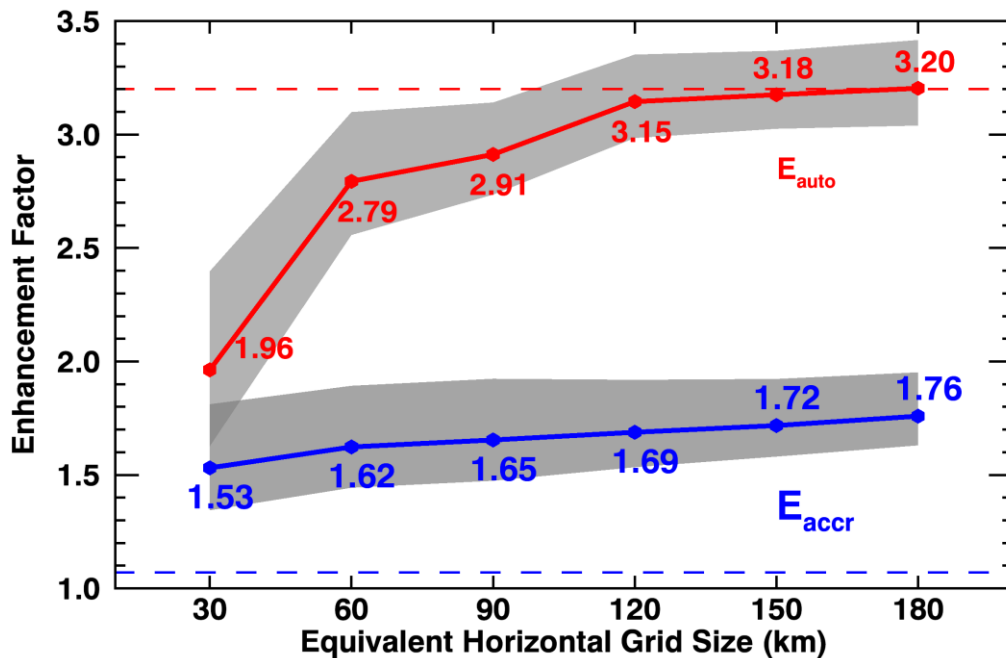
878 **Figure 2. Probability density functions (PDFs) of autoconversion (a - d) and accretion (e**
879 **- f) enhancement factors calculated from q_c (a-b), N_c (c-d), and the covariance of q_c and**
880 **q_r (e-f). The two rows show the results from 60-km and 180-km equivalent sizes,**
881 **respectively, with their average values. Black lines represent precipitation frequency in**
882 **each bin in (a)-(d) and the ratio of layer-mean q_r to q_c in (e)-(f).**

883



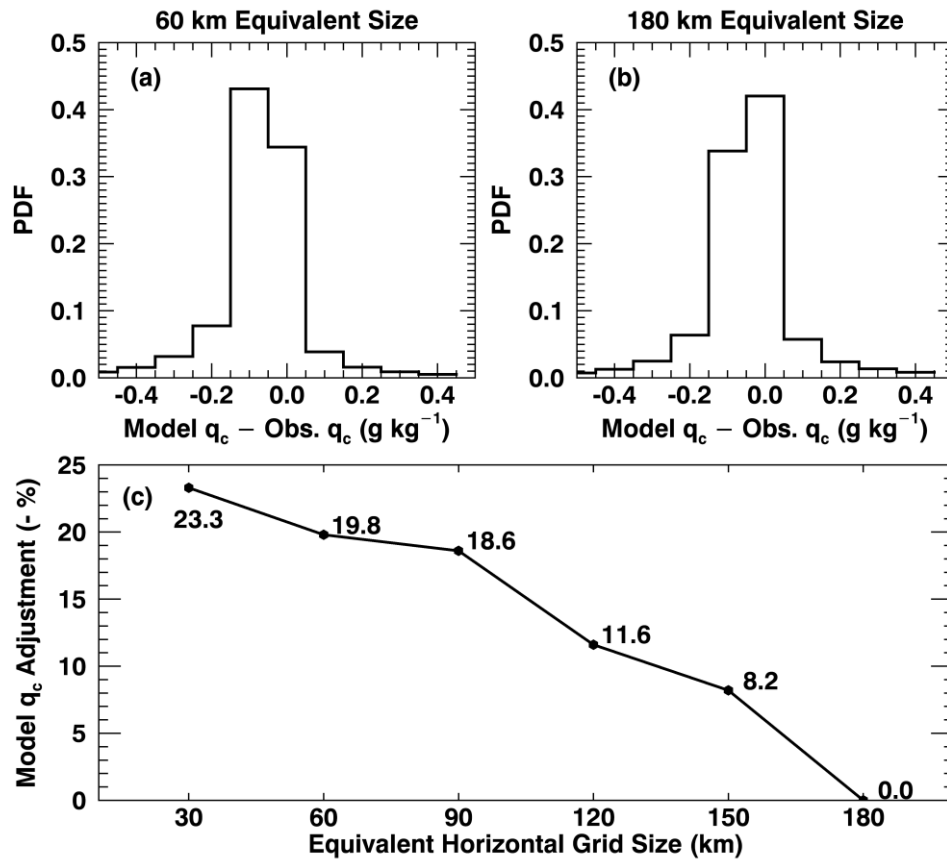
884

885 **Figure 3.** Comparison of autoconversion (a-b) and accretion (c-d) rates derived from
 886 observations (x-axis) and from model (y-axis). Results are for 60-km (a and c) and 180-
 887 km model equivalent sizes. Colored dots represent joint number densities.



889 **Figure 4. Autoconversion (red line) and accretion (blue line) enhancement factors as a**
 890 **function of equivalent sizes. The shaded areas are calculated by varying q_c and q_r within**
 891 **their retrieval uncertainties. The two dashed lines show the constant values of**
 892 **autoconversion (3.2) and accretion (1.07) enhancement factors prescribed in MG08.**

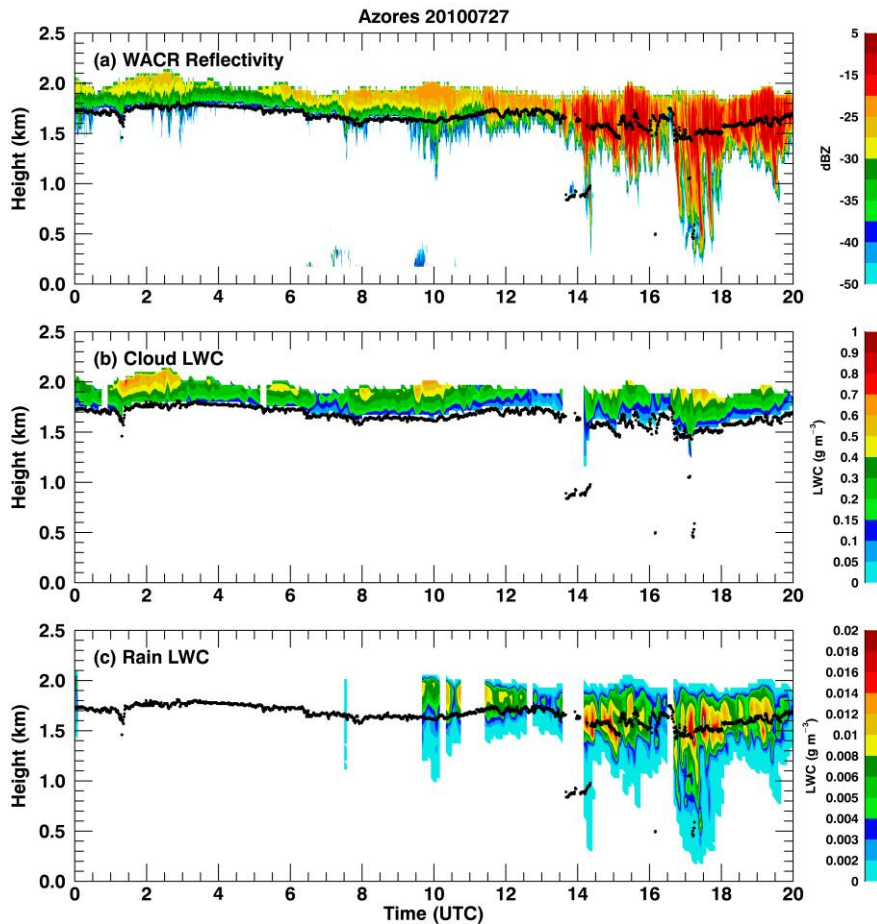
893



894

895 **Figure 5. q_c needed for models to adjust to reach the same autoconversion rate as**
 896 **observations for (a) 60-km and (b) 180-km model equivalent sizes. Positive biases**
 897 **represent increased q_c are required in models and negative biases mean decreased q_c . The**
 898 **average percentages of adjustments for different equivalent sizes are shown in panel (c)**
 899 **and note that the percentages in the vertical axis are negative.**

900



901

902 **Figure A1. Joint retrieval of cloud and rain liquid water content (CLWC and RLWC) for**
 903 **the same case as in Figure 1. (a) WACR reflectivity, (b) CLWC, and (c) RLWC. The black**
 904 **dots represent cloud base height. Blank gaps are due to the data from one or more**
 905 **observations are not available or reliable. For example, the gap before 14 UTC is due to**
 906 **multiple cloud layers ~~are detected~~—whereas we only focus on single layer cloud.**